Table of Contents for Chapter 8

Chapter 8

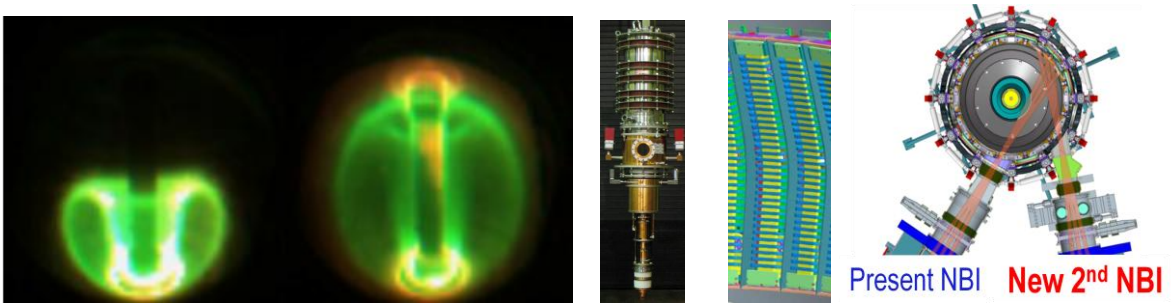

Research Goals and Plans for Plasma Formation and Current Ramp-up

8.1 Introduction

The spherical torus/tokamak (ST) configuration, due to its compact geometry and reduced surface area to volume ratio, is potentially advantageous as a Fusion Nuclear Science Facility/Component Test Facility (FNSF/CTF) by providing high neutron wall loading for nuclear component testing and development in a device significantly smaller than a full-scale reactor. However, in order to achieve low aspect ratio, the thickness of the neutron shielding of the normally conducting central magnets must be minimized, and the insulation of a conventional multi-turn solenoid will be severely degraded in the harsh nuclear environment of an FNSF. Thus, it is anticipated that future nuclear-capable STs will have little or no central solenoid capability, and that non-inductive start-up, ramp-up, and sustainment of an ST-based FNSF plasma will be required. In light of the importance of this issue, this chapter and plan is dedicated to addressing the NSTX-U 5 year plan high-level goal #3 noted in Chapter 1 to: "Develop and understand non-inductive start-up and ramp-up to project to ST-FNSF operation with small or no central solenoid."

It is important to note that conventional aspect ratio tokamaks will also require non-inductive sustainment for steady-state operation, so non-inductive start-up and ramp-up is a unique ST requirement, while sustainment is a broader tokamak/ST requirement. Further, the development of techniques to minimize or eliminate central solenoid action could also be beneficial for enabling reduced aspect ratio and/or reduced-sized superconducting electricity-producing fusion power plants [1] with reduced device mass and reduced radioactive waste production.

Given the scientific and operational challenges of non-solenoidal plasma formation and sustainment, the problem is best solved by dividing it into parts and addressing issues individually while ensuring that the pieces are ultimately compatible and can be integrated. This division of the non-inductive start-up, ramp-up, and sustainment in NSTX-U is shown schematically in Figure 8.1.

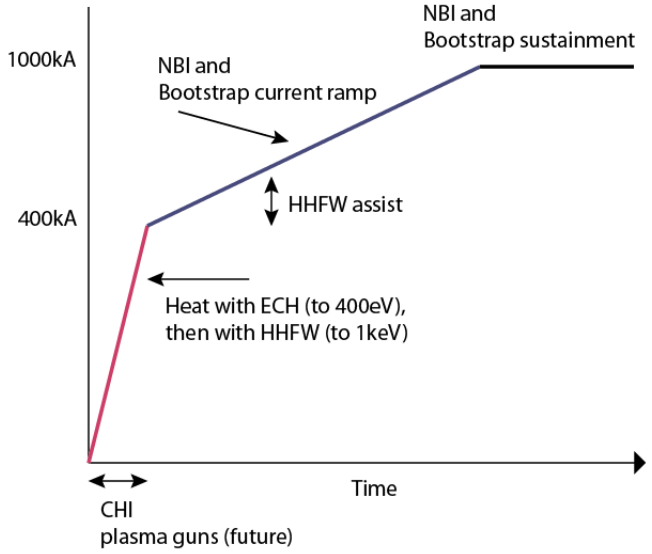

Figure 8.1: Division of plasma formation and sustainment problem into 3 distinct phases as function of time and plasma current: (1) plasma start-up, (2) initial heating and over-drive ramp-up of start-up plasma, primarily using neutral beam and bootstrap current drive and (3) sustainment of the formed plasma using neutral beam and bootstrap current drive.

Coaxial Helicity Injection (CHI), which has been the plasma start-up technique tested most on NSTX (described in Section 8.3.1) will begin operations during the first year of NSTX-U Operations (FY 2015). Plasma guns, also referred to as Point Source Helicity Injection (PSHI) (see also Section 8.3.1), is currently being developed at Pegasus at the University of Wisconsin and may undergo first tests on NSTX-U later during the 5 year plan period. These systems will be used to generate the initial seed current without reliance on the central solenoid.

A key issue for both CHI and PSHI start-up methods is that the total energy input used to form the plasma is limited in both magnitude and duration. Such plasmas are very sensitive to impurities and radiation, and while the plasma current can be high (hundreds of kA), the electron temperatures are generally low (10's of eV in the plasma core), and thus the plasma current can decay very rapidly on a 1-10 ms time-scale. This low temperature does not appear to be associated with MHD instabilities or lack of closed flux surfaces, as CHI target plasmas have been coupled to induction and subsequent H-mode transitions, can have low impurity content, and can provide significant inductive flux savings. Thus, auxiliary electron heating of the plasma to raise the central electron temperature to the 100 eV range (or higher) would be highly beneficial, as this would both reduce the current decay rate and increase the efficiency of auxiliary current drive systems used to ramp up the plasma current. Electron cyclotron heating (ECH) of a low density CHI target plasma appears very favorable for this electron heating application as described in Chapter 7, and is proposed to be used during plasma startup to significantly increase the electron temperature near the magnetic axis during CHI and plasma gun start-up. Electron Bernstein Wave (EBW) heating and current start-up has also been successfully used on MAST [2], but relative to ECH is not as well developed, and will also be tested in NSTX-U as described in Chapter 7.

High-harmonic fast-wave (HHFW) heating (also described in Chapter 7) has been used in NSTX to successfully heat a low-current (300 kA) discharge to $T_e(0) > 1$ keV in less than 40 ms [3] and generated over 70% of the plasma current non-inductively, via bootstrap current and direct fast-wave current drive, in these discharges. However, HHFW heating requires sufficient electron beta to provide sufficient first-pass absorption to heat the plasma efficiently. For typical low-current start-up plasma densities, this corresponds to electron temperatures in the ~100 to few hundred eV range. Thus, additional initial electron heating of CHI plasmas (for example via ECH) is also very likely required for HHFW heating to be effective. Further, the current drive efficiency of NBI at very low temperature is very likely too low to overcome the rapid inductive current decay of an un-heated CHI plasma. Thus, auxiliary electron heating of a CHI target plasma is also very likely required to couple to NBI current ramp-up. For these reasons, additional electron heating of start-up plasmas via 1 MW 28GHz ECH is a high priority in the NSTX-U five year plan, and heating efficiency calculations of this ECH system are shown in Section 8.5.3.

With respect to NBI current ramp-up, on NSTX, neutral beam injection (NBI) power was only well absorbed in discharges with plasma currents above approximately 600-700 kA. Further, the beams are/were not optimally aligned (are too perpendicular) for maximizing current drive efficiency, so NBI current ramp-up of the plasma current was tested to only a very limited extent in NSTX.

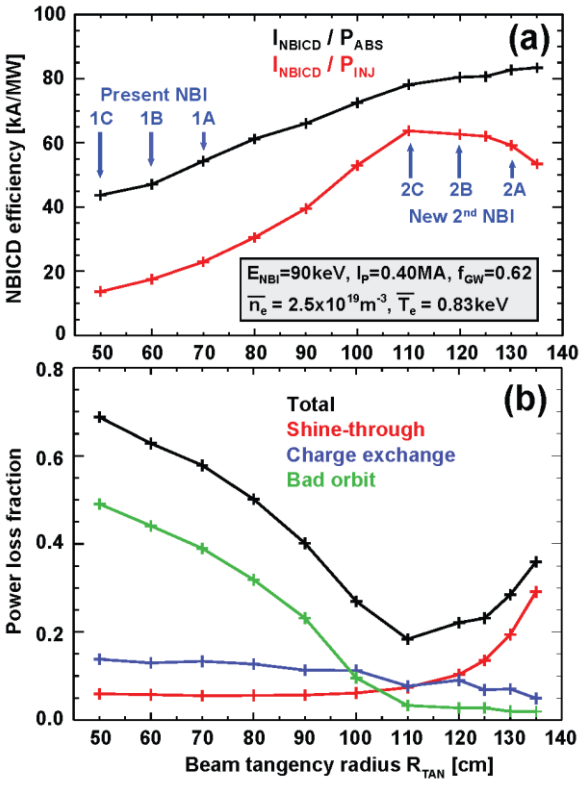

Figure 8.2: (a) NBI current drive efficiency (kA/MW) and (b) power loss fractions (total, shine-through, charge exchange, and bad orbit) as a function of beam tangency radius R_{TAN} for an A = 1.65, I_P = 0.40 MA, B_T = 0.9 T NSTX Upgrade target plasma with a 7.4 cm outer gap.

On NSTX-U, the three additional sources included in the new second NBI system of the Upgrade are aimed more tangentially and are substantially more efficient at driving current at lower plasma current. As shown in Figure 8.2 for a simulated 400 kA, n_e = 2-3×10^{19} m^{-3} and T_e = 0.8-1 keV target plasma, the new NSTX-U NBI sources (R_{TAN} = 110, 120, 130 cm) have acceptable shine-through (< 20%) and much lower bad orbit loss (< 5%) compared to the present (original NSTX) NBI sources, and 3 times higher overall current drive efficiency.

Figure 8.2 also shows that 6MW of 2nd NBI would provide 300-400 kA of current drive, and when combined with the bootstrap current of the same plasma equilibrium (also 300-400 kA) would produce current overdrive for non-inductive ramp-up. Thus, Figure 8.2 provides an initial estimate of the target plasma conditions required for efficient NBI coupling and current ramp-up of a low-current target plasma. Further, this calculation also shows that plasma temperatures in the ~1 keV range are needed for efficient NBI current drive, and this explains why initial fast-wave heating is required. Importantly, additional TRANSP simulations predict that the second more tangential NBI system on NSTX-U may be able to efficiently couple to discharges at even lower plasma currents as small as 300 kA, as described in Section 8.5.1. As will be shown later, the CHI current start-up capability in NSTX-U is expected to be at least 400 kA, providing adequate margin for NBI coupling to a CHI-generated target provided the electron temperature (and density via gas fueling) of the target plasma can be raised using wave heating such as ECH/EBW combined with HHFW. Thus, the major upgrades in NSTX-U (higher toroidal field, 2nd NBI system, and 1 MW ECH/EBW) combined with CHI generated seed current and high-harmonic fast wave heating which were already demonstrated on NSTX, appear to make possible fully non-inductive current formation and ramp-up scenarios to plasma currents up to 1 MA appear possible in NSTX-U.

To establish the predictive capability for plasma start-up in FNSF, NSTX-U research will assess the maximum levels of current that can be generated using CHI and PSHI methods. The properties of these plasmas, including plasma inductance, resistivity, electron temperature and density will be measured and compared to parameters from other machines on which they were previously developed. For CHI these are NSTX, HIT-II and possibly the HIST and QUEST STs in Japan. For PSHI this is the Pegasus experiment. These, in combination with numerical modeling, will provide scaling relations for projecting to a FNSF. These parameters will then determine the level of ECH power required to increase the electron temperature to the levels needed for direct coupling to NBI, and the required levels of NBI power needed to ramp the current to the full sustainment levels.

Numerical modeling of the full non-inductive current start-up and ramp-up will rely heavily on TSC simulations coupled to TRANSP/NUBEAM and RF codes. In addition, 3-D MHD modeling of CHI start-up and PSHI targets will be studied using the NIMROD and possibly the M3D codes to understand in detail the current formation mechanism. Then these codes will be used to understand the external control parameters (eg, operating voltage, injected flux, injector flux shaping and requirements on Z_{eff} and external heating sources) that are needed to increase the magnitude of the generated non-inductive current. Finally, the coupling of neutral beam ions to these types of plasmas will be studied both to learn the requirements on the seed current discharge properties (eg. current profile, current magnitude, electron density, temperature, Z_{eff} and the neutral beam parameters including energy, power and injection angle) that will allow the beams to more efficiently couple to the seed current targets, and for ramping these seed currents to the levels required for current sustainment.

8.2 Overview of Research Thrusts and Plans

8.2.1 Overview of Research Thrusts

The plasma formation and current ramp-up topical science group has two research thrusts. These thrusts are staged sequentially during the 5 year plan. The first thrust aims to re-establish and extend solenoid-free current start-up using coaxial helicity injection and also to test non-inductive current ramp-up using NBI plus bootstrap current overdrive – both during the first several years of NSTX-U operation. The second thrust builds on anticipated results of the first thrust, and utilizes new ECH capabilities (and PSHI if technically ready) to couple helicity-injection start-up plasmas to non-inductive current ramp-up to attempt completely solenoid-free start-up and ramp-up of an ST plasma. The thrust text is provided immediately below, background and motivation for the research plans are briefly summarized below in Section 8.2.2, and year-by-year plans are provided in Section 8.2.3. Additional technical information on start-up and ramp-up are provided in later sections of this chapter. The two research thrusts for plasma start-up and ramp-up are summarized as follows:

Thrust PSR-1: Establish and extend solenoid-free plasma start-up and test NBI ramp-up

NSTX-U researchers will re-establish transient CHI discharges utilizing graphite lower divertor tiles, the increased toroidal field capability of NSTX-U, and full Li coating of the lower divertor tiles followed by subsequent lithium conditioning of the upper divertor. The maximum toroidal currents that can be generated with CHI will be assessed by varying and increasing the amount of injector flux, the size of the capacitor bank, and the CHI voltage (up to 2 kV). The upper divertor buffer coils will be used to suppress absorber arcs, and studies of the coupling of the CHI generated plasma to inductive drive will be performed. Researchers will also generate 300-400 kA flat-top current inductive plasmas and inject the new more tangential beams to assess NBI coupling and current drive efficiency and compare to TSC/TRANSP simulations. NBI coupling to CHI targets will also be assessed and compared to simulation. Combinations of NBI and HHFW heating and current drive will be utilized to heat inductive plasmas and attempt to non-inductively ramp-up the plasma current to the ~0.8-1 MA range.

Thrust PSR-2: Ramp-up CHI Plasma discharges using NBI and HHFW and Test Plasma Gun Start-up

NSTX-U researchers will maximize the levels of CHI-produced plasma currents using new operational capabilities including 1) metallic divertor plates, 2) 1 MW 28 GHz ECH,

and 3) 2.5-3 kV CHI capability. All these should allow more injector flux to be injected into the vessel at reduced levels of low-Z impurities. Initial tests of the effectiveness of NBI coupling to a CHI-generated target will be carried out using the best available CHI targets including the expected increase in CHI plasma duration achieved with ECH electron heating, and the NBI coupling and ramp-up of CHI current will be systematically investigated. Detailed comparisons of CHI current drive results to 2D TSC and 3D NIMROD simulations will be carried out to develop a TSC/NIMROD model of CHI for FNSF design studies. If technically ready, plasma gun hardware will be commissioned on NSTX-U and point-source helicity injection (plasma gun) plasma formation will be initially tested and compared to results from Pegasus.

8.2.2 Overview of Research Plans

8.2.2.1 Solenoid-free current start-up

Three plasma start-up methods that do not rely on the central solenoid and have already shown current start-up capability on NSTX, HIT-II, Pegasus and MAST will be investigated on NSTX-U. This Chapter covers plasma start-up using CHI and PSHI. EBW start-up is described in Chapter 7.

The first method is *transient* CHI (TCHI), first demonstrated on the HIT-II ST at the University of Washington [4] and subsequently demonstrated on NSTX as well [5]. CHI is a promising candidate for non-inductive current initiation and has, in addition, the potential to drive edge current [6] during the sustained phase of a discharge for the purpose of controlling the edge current profile to improve plasma stability limits and to optimize the bootstrap current fraction. Other possible benefits include inducing edge plasma rotation for transport barrier sustainment and controlling edge SOL flows for divertor physics studies.

CHI was originally developed as part of spheromak research [7 8] and has now been used on several spheromak experiments including on the SSPX [9], CTX [10] and RACE devices [11]. Groups in US and Japan have used the method for reconnection merging research [12] and for spherical torus plasma formation [13].

CHI research on NSTX initially used the method of *driven* or *steady-state* CHI for plasma current generation [14]. Although substantial toroidal currents were generated using the steady-state approach [15], it was found that these discharges could not be successfully ramped up in current when induction was applied. Supporting experiments on the HIT-II experiment at the University of Washington demonstrated that the method of TCHI could generate high-quality plasma equilibrium in a ST that could be coupled to inductive drive [16]. Since then the TCHI method has been successfully applied to NSTX for solenoid-free plasma start-up followed by inductive ramp-up [17]. These coupled discharges have now achieved toroidal currents >1 MA using significantly less inductive flux than standard inductive discharges in NSTX.

The second method is PSHI and was first demonstrated on the Pegasus ST at the University of Wisconsin. The first version of the Pegasus PSHI system consisted of one plasma gun mounted near the lower divertor region and an anode mounted near the upper divertor region, both near the machine center stack [18]. The plasma gun consisted of a gas-injected washer stack (channel length of 2 cm) that supported an arc discharge between a cathode cup and an anode washer with an outer diameter of 2 cm [19 20]. The gun could produce large current densities (≤ 0.6 kA/cm^2) with low impurity production as long as the extracted current was less than the arc current (≤ 2 kA). Under this condition, the bulk of the injected current is extracted from the plasma arc discharge rather than from electrode surfaces.

For each discharge, external coils create an initial vacuum magnetic field such that helical field lines connect the aperture of each gun to the anode. Plasma ejected from the gun follows the vacuum field, forming helical plasma filaments. The number of toroidal transits each filament completes between the gun and anode is the geometric windup factor of the field line. At sufficiently high-injected currents, the flux surfaces rapidly heal to quiescent plasma equilibrium.

In later work, the gun's location was moved to larger radii, closer to the mid-plane of the outer vessel and similar results were obtained [21]. In these new experiments up to three small plasma guns were mounted 13—27 cm below the outboard midplane and a single anode was mounted 20 cm above the outboard midplane at the same toroidal location. In recent work, the Pegasus group has found that driving current using electrodes results in similar results [22]. Thus the present plan is to continue to develop PSHI at Pegasus to increase the level of current that can be driven during the electrode phase of the discharge (from the present ~75 kA to ~200 kA) and then during later years of the 5 year plan, if technically ready, to install and generate significant levels of start-up current in NSTX-U. These are described in Section 8.3.1.4.

8.2.2.2 Non-inductive current ramp-up

As described in the introduction, the current ramp-up requirements depend on a number of factors including both the target seed plasma parameters (including radiation losses, transport and MHD stability) as well as the tools available for current ramp-up. An ST-based FNSF is expected to rely largely on neutral beam current drive for current ramp-up. To develop a good understanding of the needs for current ramp-up, NSTX-U will study current ramp-up using a number of different seed current plasmas. These will include both inductively generated discharges as well as non-inductively generated seed current plasmas. The experimental current ramp-up requirements for these discharges that will differ in the initial current profile, density profile and temperature profile, will be compared to TRANSP simulations to develop a good understanding of both the seed current target requirements as well as the requirements on the current ramp-up systems.

Inductively generated seed current plasmas with varying current profiles will be used first to study current ramp-up using both neutral beams and HHFW. Of the three non-inductive start-up scenarios to be tested on NSTX-U (CHI, EBW and Plasma Gun start-up), only CHI will be ready

early during the present 5 year plan for a test of full non-inductive start-up and current ramp-up. The remaining two systems will be used for ramp-up studies when either has established plasma currents in the 200-400 kA ranges on NSTX-U.

8.2.2.3 Linking non-inductive current start-up to ramp-up

The first objective of any new plasma start-up method is to show that current generated by the new system is compatible with conventional inductive operation. Experiments on NSTX and HIT-II demonstrated successful coupling of CHI-initiated discharges to inductive ramp-up with significant central solenoid flux savings to reach given plasma current. CHI is incorporated into the NSTX-U design and is projected to generate over 400 kA of start-up current in NSTX-U. Similarly, the Pegasus experiment has demonstrated coupling of PSHI plasmas to induction from the central solenoid. These results show that the confinement properties of these new start-up methods are good and compatible with the conventional plasma start-up method used in all tokamaks since the inception of the tokamak concept.

CHI (and PSHI, after a suitable design of the PSHI system for NSTX-U is completed and initial current start-up up the few hundred kA established on NSTX-U), and ECH/EBW and fast-wave heating (after 200-400 kA currents are generated on NSTX-U), would be well positioned for the second and final test of the concepts, that of directly coupling to a non-inductive current ramp-up system and demonstrating that the currents could be non-inductively increased to levels required for sustained operation. Such a demonstration requires two conditions to be met: 1) The magnitude of the generated current and the plasma parameters should be adequate for coupling to the non-inductive current ramp-up system, and 2) the availability of a capable non-inductive current ramp-up system. As described in Sections 8.1 and 8.2, CHI on NSTX-U is capable of generating the required current targets needed to meet condition 1). NSTX-U will be equipped with a new ECH gyrotron, the existing HHFW system, and a new second more tangential neutral beam system that is particularly well suited for efficiently coupling to and driving current in low plasma current targets. This satisfies condition 2).

An important objective of NSTX-U is to demonstrate full non-inductive start-up and ramp-up using at least one non-inductively generated seed plasma to show that this is indeed possible, and these objectives motivate the research thrusts described above.

8.2.3 Summary of Research Plans by Year

In this Chapter, the following terminology is used in reference to Years. 'Year 1' by itself means Year 1 of the NSTX 5 year plan. 'Year 1 of NSTX-U Operations' means Year 2 of the NSTX 5 year plan, because NSTX-U will begin operations in FY 2015.

The current ramp-up studies on NSTX-U will explore two specific scenarios. These are:

(1) Bootstrap current drive: This first scenario will use discharges in which the initial plasma density is typical of the densities that exist in standard inductive discharges. These discharges will rely on HHFW for heating and driving fast wave current and also rely on bootstrap current to ramp the plasma current up. Neutral beams will also be used to provide additional current drive. This is similar to the scenarios previously studied in NSTX 300kA discharges, but these new discharges would benefit from both the increased toroidal field and higher coupled HHFW power. This scenario is also directly applicable to Advanced Tokamak scenarios.

(2) Neutral beam current drive: The second scenario will rely on discharges with densities lower than the ECH cut-off density. These will rely on initial heating by ECH and HHFW to increase the electron temperature. Neutral beams will be injected into these plasmas, and they will rely on the longer slowing down time of the neutral beam ions in the low density targets to ramp the current up. NBI current drive would be the primary component. They will also benefit from additional current drive from fast wave current drive and bootstrap current drive.

Much of the supporting work for developing these scenarios will be conducted during FY2013 and FY2014

Year 1

TSC Simulations: Develop CHI start-up scenarios for NSTX-U using TSC to support Year 2 objectives.

TRANSP Simulations: Assess NBI coupling to low current plasmas with varying internal inductance, electron temperature and electron density in support of Year 2 and Year 3 objectives.

TSC/TRANSP/GENRAY: Develop current ramp-up scenarios in support of Year 2 to Year 4 objectives. This involves simulations in which the plasma inductance, density and temperature are varied so that conditions for both bootstrap current and neutral beam driven current drive are understood.

NIMROD Simulations: Develop a model for transient CHI start-up in NSTX and begin to extend the model to the NSTX-U vessel geometry.

Year 2 (First Year of NSTX-U Operations - 2015):

Plasma start-up: Establish transient CHI discharges using graphite lower divertor tiles, using up to 0.8 T capability of NSTX-U, and full Li coating of the lower divertor tiles. Using the 2 kV capability of the CHI capacitor bank, assess maximum toroidal currents that can be generated by increasing the amount of injector flux and the size of the capacitor bank. Use the upper divertor buffer coils to suppress arcs.

CHI Coupling to induction: Couple the CHI generated plasma to inductive drive to show compatibility with inductive operation. Use a solenoid with zero pre-charge.

Ramp-up of an inductive plasma target using NBI: Generate 300 – 400 kA low density inductive plasma, with and without HHFW heating, and inject NBI from the new tangential beam system and assess NBI coupling efficiency and compare to TSC/TRANSP simulations. Based on an assessment of these results, using an inductively initiated plasma, hold the solenoid current constant and inject NBI sources. HHFW may be used to heat this plasma.

Year 3:

Plasma start-up: Improve the magnitude of the closed flux CHI produced current by using Li coating of the upper divertor to further reduce the influx of low-Z impurities. The objective is to improve on the results from the previous year and to obtain 400 kA of closed flux plasma current that is suitable for meeting the needs for satisfying Thrust 2 during Years 4-5. Compare to and improve the NIMROD simulations.

CHI Coupling to induction -1: Extending on the work from the previous year establish the flux savings that can be realized using the above plasma start-up target and with zero pre-charge in the central solenoid.

CHI Coupling to induction -2: Conduct an initial test of coupling CHI to induction using 10 – 20% solenoid pre-charge. The goal is to use some solenoid flux to increase the magnitude of the plasma current generated by CHI, but by ramping the current in the solenoid to zero, so that it can be maintained at zero during sustained non-inductive operation at this higher current level.

Assess CHI coupling to NBI: In CHI discharges that are weakly driven by induction, so as to slow down the decay of the CHI current, increase the magnitude of the neutral beam

driven toroidal current. Compare these results to TRANSP simulations to assess the neutral beam power deposition profile and neutral beam current drive.

Ramp-up an inductive plasma target using HHFW: Using a higher density 300 – 400 kA inductive plasma, ramp the current using bootstrap current over drive and increase the magnitude of the non-inductively driven current fraction. The emphasis here will be to ramp the initial current using HHFW with NBI added later during the current ramp. Use these results to improve the TSC/TRANSP/GENRAY model.

Edge current drive: To a pre-formed lower single null discharge, apply a current pulse using the CHI capacitor bank and measure the presence of any edge driven current and the resulting changes to the edge current profile.

Year 4:

ECH heating of CHI discharge: Heat a CHI iniated plasma using ECH, to demonstrate heating and a longer current decay time and provide a better target for NBI.

Plasma start-up: Maximize the levels of CHI produced plasma currents using the new capabilities that will be available during Year 4. These are (1) metal divertor plates, (2) 1 MW ECH, and (3) 2.5-3 kV CHI capability. All these should allow more injector flux to be injected into the vessel at reduced levels of low-Z impurities. If results are available from QUEST, compare with QUEST results to understand any differences between the two machines.

Couple CHI to NBI: Using the best available CHI targets, conduct an initial test of the effectiveness of NBI coupling to a CHI generated target. Results obtained with ramp-up of inductively generated plasmas (during Years 2 and 3) will determine the level of effort devoted to ramping up purely CHI generated discharges vs. additional experiments that continue to investigate NBI ramp-up of inductively generated discharges.

Couple CHI to induction: Couple to induction using the maximum possible solenoid pre-charge CHI allows. This would be dictated by the maximum amount of the central solenoid fringing fields that are compatible with CHI discharges. Ramp the solenoid current to zero, maintain the solenoid at near zero current, and test establishment of a >600 kA high temperature plasma target for use by other TSGs for sustained non-inductive operation.

Ramp-up an inductive plasma target using HHFW and NBI: Extending on the work from the previous year, discharges with both low and high internal inductance will be used as seed current targets. Extend the plasma current at which current ramp-up is initiated to lower values to assess the minimum required poloidal flux for successful current ramp-

up. Then, establish inductive plasmas with this level of poloidal flux by reducing the pre-charge on the solenoid to determine the amount of pre-charge needed to generate plasmas with the minimum required poloidal flux.

Edge current drive: Based on Year 3 results, to a pre-formed lower single null target, apply a current pulse using the DC power supplies to extend the magnitude and duration of the edge current pulse, and measure changes to the edge current profile, edge current penetration to the interior and changes to the plasma MHD stability limits and plasma transport. Use the non axis-symmetric coils to impose fluctuations to study imposed-dynamo current drive [23].

Year 5:

Plasma start-up: Maximize the levels of CHI produced plasma currents now also using the new divertor cryo pump. Validate NIMROD simulations on CHI plasma start-up using NSTX-U results and begin to develop a NIMROD model for FNSF. Compare results obtained from NSTX with other recent results from QUEST. Of the more than 300 mWb of injector flux that is available in NSTX-U determine the maximum levels that are usable and use these results for CHI design studies for a FNSF. Use these results to improve the TSC model for FNSF.

Couple CHI to NBI: Using the best available CHI targets, ramp a CHI started discharge to 0.6-1 MA using a combination of NBI/HHFW and bootstrap current over drive. Use experimental results to improve the NBI current drive model in NIMROD simulations. Validate the full TSC model (including coupling to TRANSP, NUBEAM and GENRAY) using current ramp-up results from NSTX-U.

Test plasma gun start-up: If technically ready, commission the new plasma gun hardware and test establishment of a PSHI plasma formation in NSTX-U and compare with results from Pegasus.

8.3 Research Plan

In this section we list the research plan for the five-year period. This also serves as a quick overview of the research to be conducted within the solenoid-free plasma start-up and current ramp-up topical science group. The subsequent sections provide details for the proposed work and are arranged as follows.

Section 8.3.1 introduces the reader to the transient TCHI and PSHI systems, including a brief summary of relevant previous experimental results. Section 8.3.2 describes the research plan and

detailed breakdown of the work for first two years of NSTX-U operations, which complete the task requirements for Thrust PSR-1 on current start-up and testing NBI ramp-up. Here Sections 8.3.2.1 to 8.3.2.4 describe the work to be conducted in a general manner, including supporting results from previous work. Section 8.3.3 describes the research plan and detailed breakdown of the work for Years 4 and 5 of the NSTX-U 5 Year Plan, which complete the task requirements for Thrust PSR-2 on linking current start-up and NBI ramp-up and testing point-source helicity injection. Similarly, sections 8.3.3.1 to 8.3.3.6 describe the work to be conducted in a general manner, including supporting results from previous work.

8.3.1 Overview of Helicity Injection Start-up

The primary objective of these new current start-up methods is to generate an initial seed current at a magnitude sufficient enough for directly coupling to the second more tangential neutral beam system on NSTX-U so that the current could be ramped up to the 1 MA level, which is the projected current magnitude for sustained 100% non-inductive operation in NSTX-U. To meet the requirements for coupling to neutral beams, these discharges are required to satisfy certain key confinement parameters. The first requirement is that the plasma current should be above 300 kA so that the neutral beam ions couple to these discharges. The second requirements is that the electron temperature should be sufficiently high for two reasons: 1) The higher electron temperature is required to provide the seed current discharges a sufficiently long L/R current decay time so that the neutral beam ions have sufficient time to slowdown in these discharges and drive current, and 2) the neutral beam current drive efficiency scales as the ratio of electron temperature to electron density. A third requirement is that the initial discharges should have a low electron density to ensure 2) and because it allows an efficient electron heating system such as ECH to be used as an auxiliary heating system to rapidly boost the electron temperature of these discharges to satisfy the electron temperature requirement. For NSTX-U, at a toroidal field of 1 T and for the planned 28 GHz ECH system the cut-off density for O-Mode propagation is an electron density of 5×10^{18} m^{-3}. CHI discharges on NSTX have routinely demonstrated the achievement of high-current discharges at densities of $\leq 4 \times 10^{18}$ m^{-3}.

8.3.1.1 Implementation of Transient CHI (TCHI) in NSTX-U

CHI will be implemented in NSTX-U by driving current along field lines that connect the inner and outer lower divertor plates, as shown in Figure 8.3 In NSTX-U the inner vessel and lower inner divertor plates will be the cathode while the outer divertor plates and vessel will be the anode. The configuration is very similar to that used in NSTX as described in NSTX CHI publications.

Prior to initiating a TCHI discharge the toroidal field coils and the lower divertor coils will be energized. The lower divertor coils are used to produce magnetic flux linking the lower inner and outer divertor plates, which are electrically isolated by toroidal insulators at the top and bottom

of the vacuum vessel. A programmed amount of gas will be injected into the vacuum chamber in the region below the divertor plates and voltage would be applied between these plates, as on NSTX. This will ionize the gas and produce current flowing along magnetic field lines connecting the plates. In NSTX-U initially a 5 to 100 mF capacitor bank charged up to 2 kV will provide this current, called the injector current.

The resulting current will initially flow along helical magnetic field lines connecting the lower divertor plates. The large ratio of the applied toroidal field to the poloidal field will cause the current in the plasma to develop a strong toroidal component, the beginning of the desired toroidal plasma current generation. If the injector current exceeds a threshold value, known as the bubble burst condition, the resulting ΔB_{tor}^2, ($J_{pol} \times B_{tor}$), stress across the current layer will exceed the field-line tension of the injector flux causing the helicity and plasma in the lower divertor region to expand into the main torus chamber. When the injected current is then rapidly decreased, magnetic reconnection will occur near the injection electrodes, with the toroidal plasma current forming closed flux surfaces. Figure 8.3 has a cartoon of TCHI formation in NSTX. The fast camera images in the same figure show that the TCHI discharge is fully formed about 2.5 ms after the capacitor bank is discharged.

What is note worthy is that TCHI in NSTX-U will have numerous improvements over NSTX, to be discussed in more detail in later sections, but briefly summarized here.

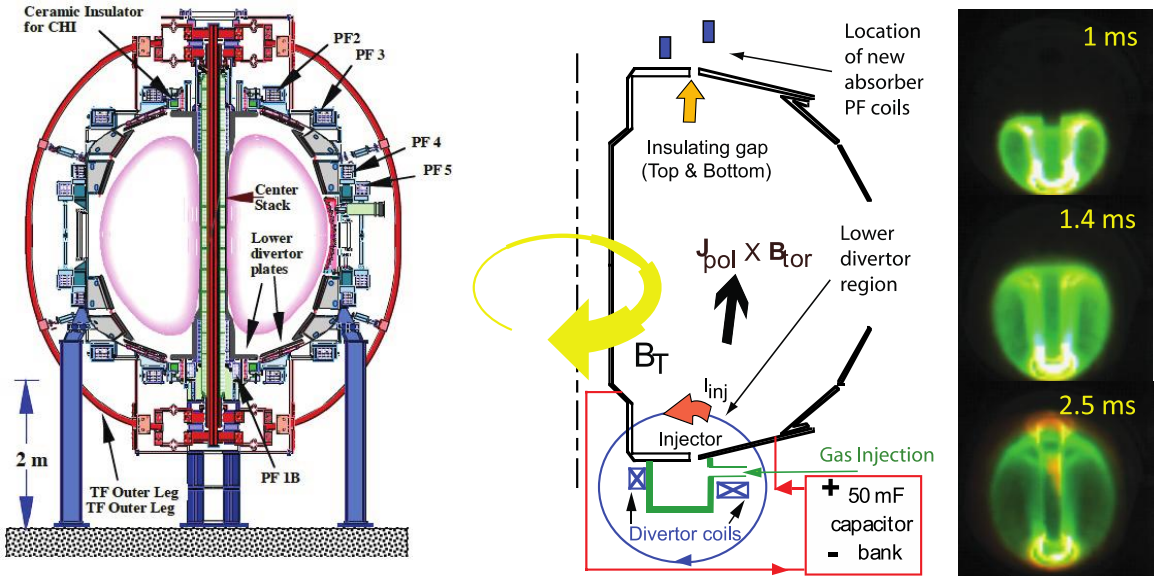

Figure 8.3: Shown are (left) drawing of the NSTX machine, (middle) cartoon of CHI start-up and (right) fast camera images of an evolving CHI discharge in NSTX 1ms, 1.4ms and 2.5ms after discharge of the CHI capacitor bank.

- The injector coil location on NSTX-U allows much better shaping of the initial injector flux because it is much closer to the gap between the divertor plates.

- The injector flux capability of the injector coils, which directly translates to the TCHI plasma current generation capability, is more than 2.5 times that in NSTX.
- The maximum toroidal field in NSTX-U will be 1 T, compared to 0.55 T on NSTX. Because of the increased toroidal flux, the current multiplication factor will proportionally increase. The current multiplication factor is defined as the ratio of the CHI generated plasma current to the injected current.
- NSTX-U is planned to be equipped with a 1 MW, 28 GHz ECH system. This will rapidly boost the electron temperature of TCHI discharges.
- The absorber coils used for absorber arc suppression on NSTX-U are also better positioned and have more than two times the current slew rates that in NSTX.
- NSTX-U will have capability for full divertor Li coating, which will further reduce the influx of low-Z impurities.
- NSTX-U will have the capability for coating the upper divertor with Li. This will reduce the influx of impurities during the occurrence of an absorber arc.
- NSTX-U will be equipped with a second more tangential neutral beam system, which is far superior to the capability on NSTX for driving current. We project, from simulations, that this should be capable of directly ramping the current produced by a TCHI discharge to the levels required for steady-state sustainment on NSTX-U.

8.3.1.2 Implications of NSTX TCHI results to NSTX-U

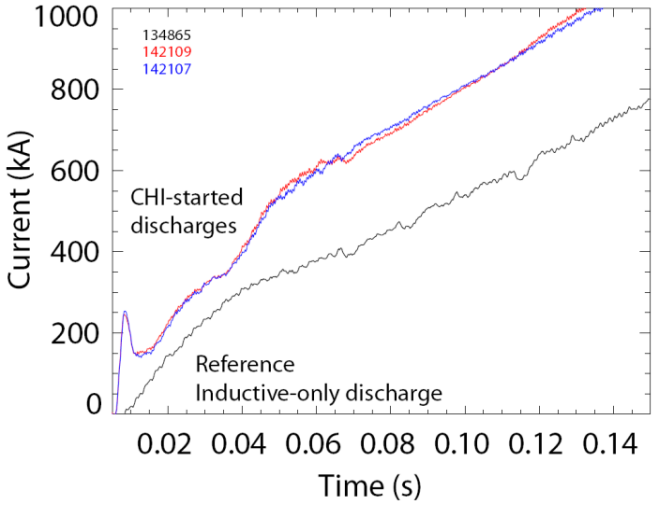

Figure 8.4: Shown are the plasma currents for two discharges initiated using CHI startup and ramped up using the central solenoid (142109 and 142107). The black trace (134865) is for a reference inductive only discharge from the NSTX 10-year database that remained in L-mode and ramped up to 1 MA in the shortest possible time. Note that at 130 ms, the CHI started discharges have ramped up to 1 MA whereas the inductive discharge that has used the same amount of inductive flux has ramped to a lower value of 700 kA.

Figure 8.4 shows two CHI started discharges that were coupled to induction. The third discharge is an inductive-only case that is a non-CHI discharge from the NSTX database (assembled over 10 years of operation) that reached 1 MA in a shorter time than other L-mode discharges. For the CHI initiated discharge at 132 ms, a total of 258 mWb of central solenoid flux was required to ramp the discharge to 1 MA. The non-CHI discharges at this time only get to about 0.7 MA and do not reach 1 MA until 180 ms, by which time 396 mWb of central solenoid flux had been consumed. Thus, the L-mode discharges from the NSTX data base

require at least 50% more inductive flux than discharges assisted by CHI. The inductive-only discharge on NSTX that consumed the least amount of solenoid flux to reach 1 MA, among all the discharges in the NSTX data base, transitioned to an H-mode. That discharge required 340 mWb to reach 1 MA, which is still significantly higher than the CHI started discharges.

In Figure 8.5, we show other parameters for discharges started with and without CHI [24]. The CHI assisted discharges have much lower plasma internal inductance and their line-integrated electron density is about one half that of the standard NSTX discharges. As a result of the lower inductance, the CHI started discharges also have a higher plasma elongation for a similar programming of the NSTX shaping coils. The CHI assisted discharge 142140 has a higher electron density than discharges 140872 and 140875, starting from 80 ms, due to increased gas puffing.

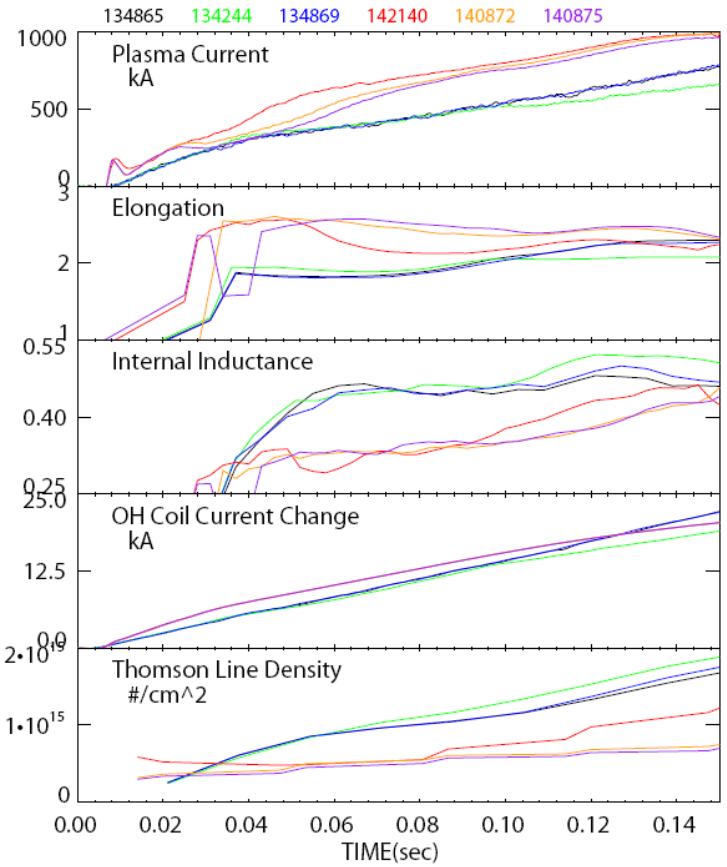

Figure 8.5: Shown are from top to bottom, time traces for the plasma current, plasma elongation, normalized plasma internal inductance, current change in the central solenoid and the electron line density from a Thomson scattering diagnostic. The traces are for three discharges initiated using CHI startup (142140, 140872 and 140875) and three reference inductive-only discharges from the NSTX 10 year database that ramped to 1 MA in the shortest possible time.

We note from the traces showing the difference in the flux change produced by the central solenoid that initially the CHI started discharges consume more inductive flux. For the CHI started discharges the initial loop voltage is about 3 V for 20 ms while the plasma current is about 200 kA, which results in a modest input power of 600 kW. In future devices auxiliary heating power of this magnitude for about 20 ms, such as from Electron Cyclotron Heating, should be able to boost the electron temperature and reduce plasma resistivity. However, past this initial time, the loop voltage consumed by the CHI discharge drops below the level in the non-CHI discharge. At about 120 ms, the inductive flux used by both discharges becomes equal. Beyond 120 ms, the flux usage by the CHI discharge drops rapidly because the CHI discharge uses a unipolar central solenoid swing with a maximum

available flux of 330 mWb. The non-CHI discharges use a bipolar swing and so have twice as much flux available (660 mWb). At 150 ms, the loop voltage for the CHI started discharges becomes too low to sustain these 1 MA plasmas. The drop in the applied loop voltage is also the reason for the gradual increase in the internal inductance after 120 ms.

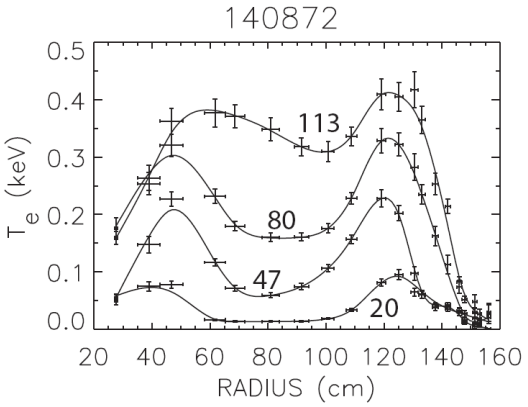

Figure 8.6: T_e profiles at t = 20, 47, 80 and 113 ms for a CHI started discharge that was inductively ramped up. The initial hollow T_e profile is retained during the current ramp.

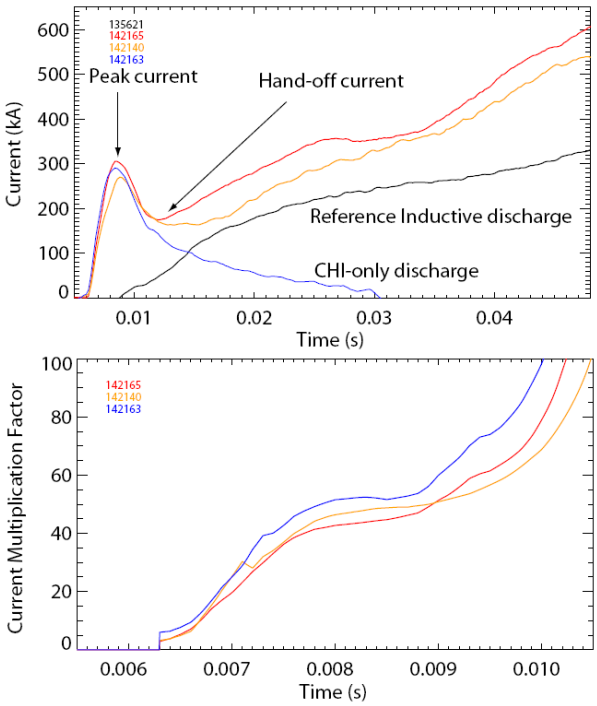

Figure 8.7: Top – Plasma current traces for a CHI-only discharge (142163), CHI started discharges that were ramped up using induction (142165 and 142140) and for a reference inductive-only discharge that had the same inductive loop voltage programming as the CHI discharges that were ramped up using induction. Note that the initial peak startup currents are 300 kA and when ramped using induction, the CHI started discharge ramps up to over 600 kA whereas the inductive-only discharge reaches about 300 kA. Bottom – shown are the current multiplication factors for the three CHI-started discharges.

Operational experience has shown that for the standard inductive startup in NSTX, both the higher plasma density and the slower current ramp rates of the discharges in Figure 8.5 are required to avoid MHD instability during the current ramp. The CHI started discharges seem immune to this, however, although the reasons for this are not known at this time. It could be related to the hollow electron temperature profile, shown in Figure 8.6, that is characteristic of CHI startup [25]. Initially CHI drives all current in the edge region of the plasma. After flux closure it could then be expected that most of the current would still flow at the edge until current relaxation causes the edge current to diffuse to the interior. This initially hollow current profile should result in a higher edge temperature and relatively cooler plasma center. This is indeed seen in the CHI started discharges as shown in Figure 8.6. This hollow electron temperature profile persists during the subsequent inductive ramp, which causes more of the current to flow in the outer region resulting in lower inductance plasma. The lower inductance is favorable for achieving high elongation of the plasma cross-section as the plasma current is then

closer to the equilibrium control coils. That CHI started discharges naturally provide this plasma configuration is a desirable feature for developing advanced scenarios.

Another beneficial aspect of the CHI started discharges is their lower electron density. Because the energetic neutral-beam ions take a longer time to slow down in lower density discharges, the neutral beam current drive fraction increases. Low-density targets are thus a requirement for ramping up an initial current to higher current levels with NBI. In this scenario, NSTX-U will rely on reduced density to increase the neutral beam current drive fraction during the initial current ramp-up phase [26].

Figure 8.7 shows a representative CHI-only discharge (142163) that attained a peak current of 0.3 MA and two similar discharges (142140, 142165) with induction also applied. The fourth discharge (135621) is an inductive-only discharge that used the same loop voltage programming as discharge 142165. By about 45 ms, the CHI started discharge reaches a current about 0.3 MA more than the reference inductive-only discharge. The initial energy stored in the capacitor bank was 29 kJ resulting in a current generation efficiency of over 10 Amps/Joule. The current multiplication factor defined as the ratio of the plasma current to the injector current is over 50.

8.3.1.3 Increased TCHI current start-up capability in NSTX-U

CHI started discharges that have induction applied, both on HIT-II and on NSTX generally show a drop in plasma current before the current eventually begins to ramp-up. The lowest current during the current ramp is referred to as the hand-off current, as shown in Figure 8.7. The magnitude of this drop can be as small as 10% but generally it is about 30%. There are two reasons for this. The first reason is due to the plasma resistivity. Reducing the impurities further would reduce the plasma resistivity through decreasing the Z_{eff} and reducing the radiated power that decreases the electron temperature. Auxiliary heating could also overcome the effects of any residual low-Z impurities.

The second reason for the current drop is a change in plasma inductance as the initially hollow, and therefore low inductance, current profile naturally relaxes. This current profile relaxation is simply resistive diffusion of current. The ratio of the initial peak current to the hand-off current provides an estimate of the initial inductance of the CHI started plasma at the time of peak startup current. Soon after coupling to induction the normalized plasma internal inductance of about 0.35 as computed by the EFIT code for these discharges is maintained through most of the inductive ramp, until the loop voltage becomes too small to sustain the plasma current. The poloidal flux corresponding to this plasma inductance is given as,

$$\psi_p = I_p R_p l_i \mu_0 / 2 \qquad (1)$$

Substituting l_i = 0.35 and I_p = 165 kA, and the EFIT computed value of the plasma major radius R_p = 0.87, Eq. 1 gives ψ_p = 31.5 mWb. In the absence of flux amplification this is the amount of poloidal injector flux that must be injected into NSTX. Assuming that there is no poloidal flux

decay due to resistive loss, the initial plasma internal inductance at the peak toroidal current of 270 kA is then 0.21 for these discharges.

We can now calculate the current multiplication factor using two different methods. In the first method, we use the poloidal flux calculated by Eq. 1. In the second method we use the experimentally measured plasma and the injector currents.

The plasma enclosed toroidal flux for NSTX at 0.55 T is 2.68 Wb. From Eq. 1 the calculated poloidal flux is 31.5 mWb. The current multiplication factor calculated as the ratio of the toroidal to poloidal flux,

$$CM = \phi_T/\psi_p \qquad (2)$$

is 85, which is roughly consistent with the measured current multiplication in NSTX, which is in the range of 50 to 100.

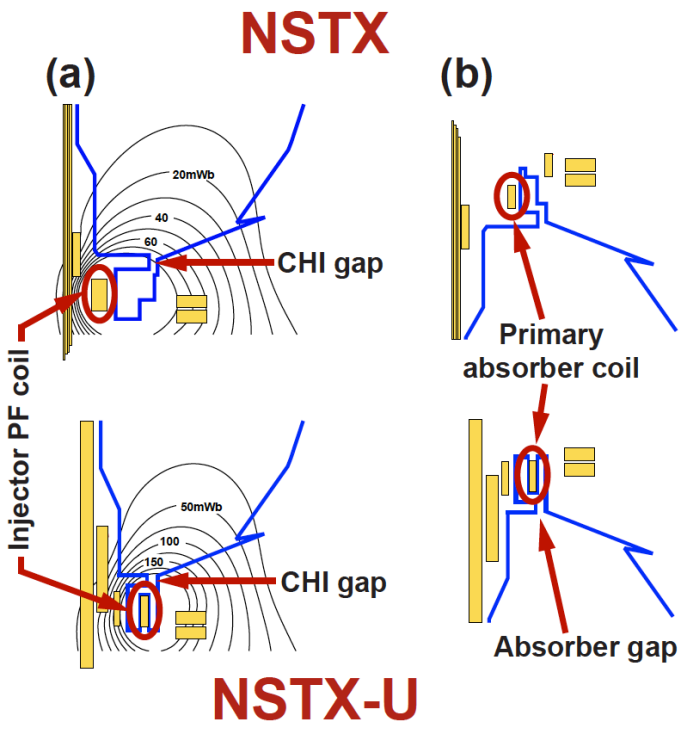

Figure 8.8: Shown are the locations for the injector and absorber PF coils on NSTX (Top) and for NSTX-U (Lower figures). Note that on NSTX-U there are two injector coils. Use of both coils would increase the injector flux to over 300 mWb.

The experimentally measured current multiplication is calculated as the ratio of the plasma current to injector current as:

$$CM_{Exp} = I_p/I_{inj} \qquad (3)$$

For discharge 142140, this current multiplication factor is about 60. A likely reason for the higher current multiplication factor that is obtained from the poloidal flux calculation using plasma inductance is that between the time of peak plasma current and the hand-off current some of the injected poloidal flux has decayed away. These calculations also assume that there is no dynamo activity that generates additional poloidal flux. If there is flux amplification, then the poloidal flux calculated using Eq. 1 would exceed the injector flux calculated using experimental poloidal flux loop measurements. Flux amplification would result in the generation of more toroidal current than can be accounted for by the amount of injected flux.

The injected poloidal flux based on external magnetic measurements varies between 30 and 50 mWb depending on the calculation method. The higher value is the difference in measured

poloidal flux between poloidal flux loops located on the outer edge of the inner divertor plates at the top and bottom of the machine. This provides an upper bound. The lower value is the difference in poloidal flux between poloidal flux loops located at the inner and outer edges of the outer divertor plate, which provides a lower bound. The range of experimental flux measurements is consistent with the poloidal flux calculation using plasma parameters in Eq. 1.

Parameters	**NSTX**	**NSTX-U**
R(m)	0.86	0.93
a(m)	0.68	0.62
B_0(T)	0.55	1.0
Toroidal Flux (Wb)	2.68	3.78
Normalized internal inductance, *l*i	0.35	0.35
Full non-inductive sustainment current, Max Ip (MA)	0.7	1
Poloidal Flux for Max Ip (mWb)	132	206
Required Injector Flux for 50% Max Ip (mWb)	66	103
Current Multiplication factor	41	37
Peak current multiplication	53	48
Peak startup current (kA)	450	650
Injector current	**8.6**	**13.6**
Maximum available Injector Flux (mWb)	63-80	220-340
Max startup current potential (kA)	~400	~1 MA
Required injector current For Max current potential (kA)	10	27*

*Table 1: CHI startup parameters in NSTX and NSTX-U (*HIT-II routinely operated with 30kA injector current without impurity issues)*

Using these equations we can now calculate the projected values of the current multiplication factor and the toroidal current CHI could generate in the NSTX-U. The device parameters and the calculated values are listed in Table 1.

First we assume that CHI will be capable of generating discharges with a normalized internal plasma inductance of about 0.35, as on NSTX, which is a reasonable assumption. The planned level for fully non-inductively sustained plasma currents in NSTX-U is 1 MA. For these conditions, Eq. 1 results in an enclosed poloidal flux of 206 mWb. Because in NSTX, the EFIT calculated value of the plasma major radius is very close to the machine major radius of 0.86, we have here assumed that R_p for NSTX-U in Eq. 1 is equal to 0.93.

For CHI plasma startup at a current level of about 500 kA the enclosed poloidal flux in NSTX-U is reduced to 103 mWb. For this condition, using Eq. 2, we can calculate the current multiplication factor in NSTX-U to be equal to 37. Based on the hand-off current magnitude of 500 kA and this value of current multiplication the required injector current, calculated using Eq. 3, is 13.6 kA. Because of an initial lower inductance, the peak CHI produced toroidal current could be expected to be higher than the hand-off current by about 30%, as described before. The peak toroidal current and the current multiplication factor could be expected to be 650 kA and 48 respectively. TRANSP analysis suggests that the second more tangential neutral beam system on NSTX-U may be capable of coupling to discharges with a plasma current as small as 300 kA. Based on results from NSTX and projection to NSTX-U, CHI should be able to generate currents well above this level.

Based on vacuum field calculations for NSTX and NSTX-U, we note that the available injector flux for NSTX-U is considerably more than the enclosed poloidal flux in a 1 MA NSTX-U discharge. This significantly improved current generation potential in NSTX-U is due to the much-improved design of the CHI injector flux coil, which is positioned much closer to the CHI insulating gap. Note from Figure 8.8 that the injector coil in NSTX is much farther away from the insulating gap, resulting in a much smaller amount of the flux generated by this coil that usefully connects the inner and outer divertor plates. The much larger range for the injector flux in NSTX-U is due to the provision of two injector coils. The lower limit on the injector flux assumes that only one of these coils (the primary coil) would be used and the flux is calculated using the second method described above. The upper bound on the injector flux uses both injector coils and the injector flux is calculated using the first method.

Although the injector flux capability in NSTX-U is large, the amount of useful injector flux defined as the amount of flux that can be injected with acceptable amounts of low-Z impurities may be determined by electrode conditions. This is because a larger value of injector flux requires a higher level of injector current [27] and the higher current densities on electrode surfaces would increase the amount of impurity influx. Present NSTX experiments that have a graphite inner divertor electrode have been able to achieve injector current as large as 10 kA and these discharges when coupled to induction have successfully ramped to 1 MA. So this could be assumed to be a lower injector current bound on NSTX-U. Because the toroidal field on NSTX-U is nearly twice that in NSTX, the same value of injector current can inject nearly twice the injector flux in NSTX-U. This should result in a lower bound on CHI produced toroidal current in NSTX-U on the order of 0.5 MA. If the injector current can be increased without creating additional impurity influx, CHI-generated toroidal currents in excess of 1 MA are theoretically possible in NSTX-U. With better electrode surfaces, HIT-II TCHI discharges routinely operated with injector currents of 30 kA without impurity issues [28]. NSTX-U plans to implement metal divertor plates. This in combination with more complete coverage of Lithium on divertor surfaces and ECH capability should allow NSTX-U to operate at injector currents well above the 10 kA achieved on NSTX.

8.3.1.4 Point source helicity injection (PSHI) plasma start-up

Local helicity injection is a non-solenoidal current drive technique, similar in concept to CHI, except that the injector is relatively compact and can be located anywhere at the plasma boundary. Current is driven on open field lines at the tokamak edge, injecting both power and magnetic helicity, and over time MHD activity incorporates this increased magnetic helicity as an increase in the toroidal plasma current. Experimental studies in Pegasus have demonstrated the formation and growth of more than 170 kA of plasma current, using only 4 kA of driving open-field-line current [29]. This technique appears to be scalable to a device of the scale of the NSTX-U, and the conceptual design of a 1 MA startup system for NSTX-U is presently under development in an external collaboration with the Pegasus team. This collaborative activity encompasses the materials and technology in any deployed NSTX-U injector, a deeper

understanding of the physical processes that guide the injector design, pre-deployment conditioning and testing of the NSTX-U injector and associated power systems, and development of realistic operating scenarios for helicity injection startup to the 1 MA level on NSTX-U. The system is currently being developed at Pegasus and it is envisioned that the full design would be completed during the first two years of the NSTX-U 5 year plan. The system may be ready for installation in NSTX-U during Year 4, with tests up to the 0.5 MA conducted during Year 5.

8.3.1.5 PSHI Results from Pegasus

Past studies of compact helicity injection in Pegasus used an array of compact active PSHI guns to form an axisymmetric but turbulent plasma equilibrium. Substantial ramps in the outboard poloidal field coil currents provided both inductive current drive and radial force balance as the toroidal plasma current increased. MHD activity and the induction have been shown capable of driving up to 170 kA of toroidal plasma current, using only 4 kA of bias current on open field lines. Detailed analysis shows that the vast majority of the current drive in these scenarios is actually from the induction, especially during the high-current phase of the plasma evolution [30]. Although induction-driven scenarios are an effective demonstration of this non-solenoidal startup technique, the strong reliance on induction presents significant limitations. Note, the quantity of Volt-seconds available to induction is limited, which may prevent the technique from successfully driving high-current startup plasmas in the presence of strong dissipation (e.g., high impurity content). Also, the strong outer poloidal field (PF) ramp greatly complicates the radial position control problem, as the dominant drive for the plasma current is also the vertical field. For these reasons, efforts have been recently directed at the development of hardware and operating scenarios in which the helicity injection current drive dominates over any inductive effects from changes in the vertical field. Proof-of-principle demonstration discharges, in which the helicity injection is providing nearly all of the current drive, have been formed and sustained in the Pegasus tokamak, and further development is ongoing.

In terms of the technological development, major strides were made in the past year at the Pegasus facility in developing a viable large-area electrode assembly integrated with one to three active plasma gun current injectors. After tests with both graphite and Mo electrodes, the Mo structure was found to best handle the high heat load and high extracted current density required for an injector.

A local scraper limiter concept was successfully tested to control the density in the injector vicinity and reduce plasma interactions with the injector hardware in the scrape off region. Electrode geometry was developed which both insulates the injector in front of a boron-nitride (BN) insulator assembly and reduces excessive plasma interactions with the BN hardware. This assembly showed reduced impurity generation, to almost negligible levels in the bulk tokamak plasma.

Studies on Pegasus over the past two years have shown that the impedance of the edge current sources is very sensitive to the gas-fueling rate through the plasma gun injectors. It appears that a fast-varying gas flow rate and different flow rates for the passive electrode and active gun sources will be required to optimize the helicity injection rate. To that end, an integrated single-gun, extended electrode injector assembly with a fast piezo-electric gas feed has been designed and installed in Pegasus for testing. It includes the material and geometry advances noted above. Together, this integrated assembly provides a first generation conceptual design for a possible injector assembly that may be deployable to NSTX-U.

Finally, a test electrode assembly has been installed in the divertor plate region of Pegasus to provide initial tests for optimizing the tradeoffs between increased helicity injection in the high-field region near the centerstack and some poloidal induction current drive available from injection in the low-field side outer plasma region. Results from these tests will be integrated with the modeling to suggest optimal geometries for deployment on NSTX-U.

New power systems are under development for the helicity injection systems on Pegasus, and these will provide prototype tests of concepts for power systems on NSTX-U. A new single-quadrant H-bridge assembly has been developed for the bias voltage power supply, which drives the current into the plasma chamber. This system has the advantage of high-voltage (~ 2 kV) and high current (~14 kA) with a single solid-state switch assembly. It promises higher reliability and more robust fault protection than the 4-quad assemblies used earlier in Pegasus. This system will be tested in helicity drive operations in the next year on Pegasus. Incremental improvements in the safety features of the plasma gun arc systems have also been deployed, and should be transferable to the eventual NSTX-U design concepts.

8.3.1.6 Proposed PSHI hardware and access for NSTX-U

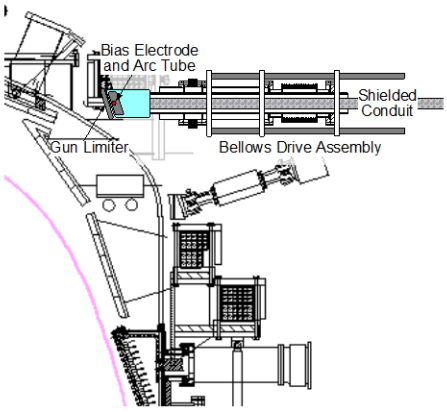

Figure 8.9: NSTX/NSTX-U cutaway, with pre-conceptual injector.

The conceptual design for the NSTX-U PSHI is presently under development, and will be finished in FY2014. What follows is based on a particular pre-conceptual design for the startup system, and is broadly consistent with the developing parameters and features of the final conceptual design.

Figure 8.9 shows a partial cutaway of the NSTX-U vessel with the pre-conceptual injector structure superimposed, to illustrate the scale and location for any eventual compact injector. Machine access would be through a large (8-inch diameter or larger) off-midplane port on the outboard side. The injector will be designed to be fully retractable, using a bellows drive for vacuum integrity, and will be kept outside the NSTX-U vessel and behind a gate valve (in a "garage" region) when

not in use. The plasma-facing portion of the injector will incorporate a limiter structure, an active plasma gun (the arc tube), and a passive electrode. The electrode will be shaped, as much as possible within the footprint of the port, to maximize the Taylor limit [31] while keeping an adequate cross-section for the corresponding current drive. The umbilical cables, tubing, and diagnostic lines from the injector to the power supplies and control system will be kept in a shielded conduit, both to isolate the diagnostic lines from external noise sources and to mitigate the electrostatic noise associated with high-power switching of the injector H-bridge bias supply. Deuterium gas for the active plasma gun is supplied through flexible tubing, with most fueling during the electrode-drive phase supplied through the usual NSTX-U fueling valves.

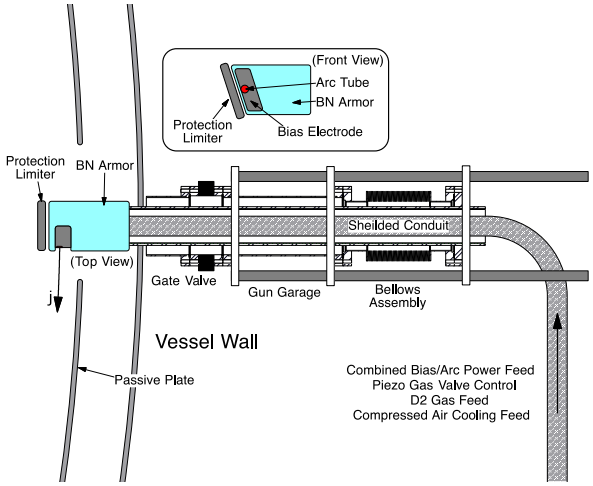

Figure 8.10: Detailed view of pre-conceptual design.

Figure 8.10 shows a more detailed top-down view of the proposed injector, with explicit detail of the gate valve, injector "garage", bellows structure, and the umbilical cables and tubing. The injector is shown inserted between two passive plates, though those details are dependent on the exact port that is made available on NSTX-U for these studies. A more detailed insert shows the elements of the pre-conceptual injector, including the limiter, the arc tube surrounded by an electrode, and an insulating surface behind the electrode to prevent arcing back along the field lines. The present design uses boron nitride as both the insulating surface and the plasma-facing armor for the sides of the injector. The final conceptual design may well use molybdenum or tungsten armor around and behind the injector, in order to shield the boron nitride from plasma impact.

The power supplies and control system can be relatively compact, depending upon the total stored energy that will be necessary for driving the bias during the high-current startup scenario. A simple pulse-forming network will provide the arc discharge in the active plasma source, with a crowbar switch on the outputs to the arc tube. The bias power supply will be based on the technology used on Pegasus, with an array of reduced H-bridge supplies providing the required current and voltage. The arc supply, bias bridges, deuterium gas supply, and control systems will perhaps occupy the volume of an office desk. The total stored energy for the bias supply, necessary for a high-current startup scenario, remains to be determined.

8.3.2 Thrust 1 Research Plans (Years 1 to 3): Establish and Extend Solenoid-free Plasma Start-up and Test NBI Ramp-up

The goals for TCHI plasma start-up will be to first establish plasma start-up in the new vessel configuration, test the capabilities of the CHI hardware such as the new injector and absorber coils, relying on increased Li coverage capability and to ramp a CHI plasma using induction. In other experiments 300-400 kA inductively generated plasma will be ramped-up in current using HHFW and neutral beams. In support of this work, simulations using TSC, TRANSP, GENRAY and NIMROD codes will be conducted during Year 1, as outlined in Section 8.2.3, and discussed further in Section 8.5.

In the area of plasma gun start-up, development work will continue at the Pegasus facility as described in Section 8.3.1 aimed at finalizing the hardware specifications for implementing the PSHI capability on NSTX-U after the system is ready.

8.3.2.1 Use graphite divertor plates with full Li coverage, improved absorber PF coils

During the first two years of NSTX-U operations, NSTX-U will be configured for operation with graphite divertor plates. Initial discharge development on NSTX-U will therefore use the graphite divertor plates as the CHI electrodes. This has the benefit of touching base with previous results from NSTX and assessing in more detail the benefits of full Li coverage and the resulting increases in injector current that can realized on NSTX-U. This also then allows for comparison of the results with full metallic divertor plates during years 4-5.

Significant progress was possible as a result of dedicated efforts to reduce the influx of low-Z impurities in NSTX using methods such as divertor surface conditioning using long-pulse CHI discharges, absorber arc suppression using absorber poloidal field coils and through the use of Li evaporative coatings. This allowed the CHI plasma temperature in NSTX, for the first time, to reach 50 eV in parts of the CHI discharge. This was a significant step as these improvements allowed record levels of start-up currents, up to 300 kA, to also be generated by CHI in NSTX that were then successfully coupled to induction with the realization of central solenoid flux savings.

In CHI terminology the lower part of the vessel from which poloidal flux is injected is called the injector region. The opposite end of the machine is referred to as the absorber region, because the E x B drift is away from the injector region and into the absorber region. During CHI operation if the expanding CHI plasma makes adequate contact with the absorber end of the machine, then it is possible for the injected current to flow along the vessel and bridge the insulator gap at the absorber end of the machine. This is a condition to be minimized, as it can introduce low-Z impurities in to the plasma.

An example of the dramatic benefits of reducing low-Z impurities in a CHI discharge is illustrated in Figure 8.11. Both discharges in this Figure benefitted from similar level of Li conditioning. One of the discharges benefitted from the use of absorber coil, shown in Figure

8.8. Energizing this coil generates a local magnetic buffer field. This has the consequence that this buffer field holds the expanding CHI discharge back from contacting the upper divertor plates. Discharge 135622, which has no current in the absorber buffer field coils, shows no coupling to induction for otherwise identical conditions. An examination of the injector current trace shows the characteristic spike at 9 ms, indicative of the occurrence of an absorber arc. The occurrence of the absorber arc is also seen as a bright ring around the top of the center column in the fast camera image at 8.5 ms. On the other hand, the discharge 135616, with buffer field applied, does not have the absorber arc and the CHI-produced discharge couples well to induction and ramps up to 800 kA. Note that both discharges show nearly identical fast camera images just prior to the occurrence of the arc at 7.5 ms. At 20 ms, the discharge with the absorber arc shrinks in size and is still radiating in the visible spectrum whereas the discharge with no arc, because of its higher temperature is no longer radiating in the visible spectrum.

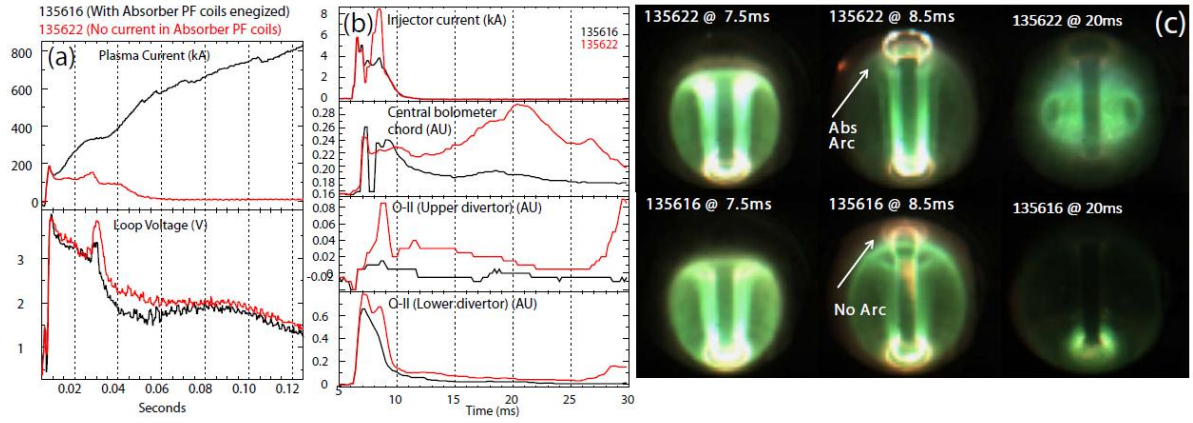

Figure 8.11: Shown are (a) the plasma current and pre-programmed loop voltage for two discharges. Discharge 135622 is a reference discharge in which the absorber PF coils were not energized. In discharge 135616 the absorber PF coils provided a buffer flux to the expanding CHI discharge. Also shown are (b) the injector current, signal from a central chord bolometer, the upper and lower divertor O-II signals. (c) The right column contains fish-eye camera images just prior to, during and after the absorber arc for both discharges.

Traces for the oxygen line radiation signatures show that although the lower divertor oxygen levels are nearly the same for both cases (due to similar levels of Li conditioning), a dramatic increase in the upper divertor oxygen signal is seen when the absorber arc occurs. The central chord bolometer signal also shows significantly elevated levels of radiated power well after the absorber arc has ceased, indicating the presence of increased amounts of low-Z impurities, as is also apparent in the upper divertor oxygen signal.

An added benefit of reducing the low-Z impurities has been that for the first time in NSTX, the electron temperature in the CHI discharges remains above 20 eV (reaching 50 eV in parts of the discharge) as the size of the capacitor bank is increased. Now the additional capacitor bank energy is contributing to heating the plasma, rather than being lost as impurity line radiation, as was the case in previous experiments on NSTX. We have seen this behavior on the HIT-II experiment as well that show that the highest plasma currents are produced immediately after

titanium wall conditioning is used. Thus on NSTX-U further controlling the low-Z impurity influx should allow the plasma electron temperature to increase and also contribute to increasing the magnitude of the initial start-up current. Such future discharges could also be expected to have longer L/R current decay times.

8.3.2.2 Test benefits of (partial) upper metal divertor and Li during absorber arcs

It was noted in the previous section that contact of the evolving CHI discharge with the upper divertor plates resulted in an influx of impurities (Oxygen) that subsequently degraded the performance of the CHI discharge. In addition to the absorber buffer field coils, another method for controlling low-Z impurities, which has not been used thus far, is to use lithium conditioning of the upper divertor plates. It is seen from Figure 8.11 that that soon after the CHI plasma contacts the upper divertor the O-II signal from the upper divertor increases and the discharge subsequently runs into a radiation issue. One of the reasons for this could be because NSTX is routinely operated in a lower single null configuration or a double null that is biased towards the lower divertor. During the final two years of NSTX operations, NSTX did not have significant dedicated experiments in the upper single null configuration. Thus the upper divertor never gets adequately used and has more surface impurities. Thus it is conceivable that if plasma contacts the upper divertor, surface contaminants would enter the discharge. Also, the usual Li evaporative coatings on NSTX direct a plume of Li towards the lower divertor surfaces and none of this Li coats the upper divertor. So in addition to not being conditioned by plasma discharges the upper divertor also does not benefit from Li coatings.

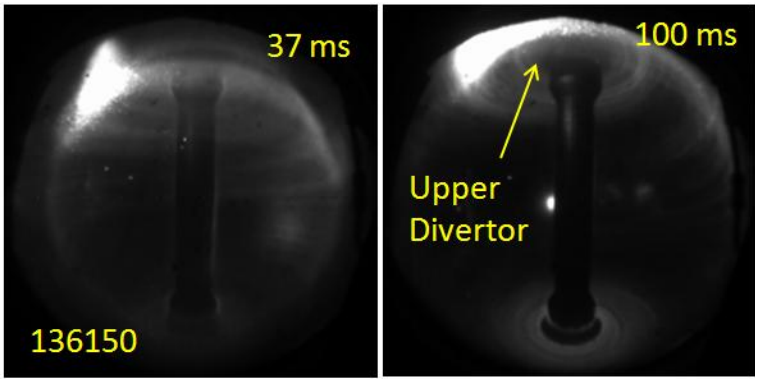

Figure 8.12: The image on the left shows Li powder being dropped on to the top of a NSTX discharge. The image on the right shows the ionized powder being transported towards the upper divertor.

An observation in past experiments that used the Lithium Dropper system [32] was that, when the Li powder was dropped on to a weakly upper biased double null discharge (produced during the FY09 reversed B_T campaign) the ionized Li is transported towards the upper divertor region and presumably coats the upper divertor. A visible camera image of this is shown in Figure 8.12. Thus, if a few of these discharges are run prior to a CHI discharge, then, in the event that the top of a CHI discharge contacts the upper divertor, possibly less oxygen and other surface contaminants, would enter the discharge. While this could be tried on NSTX-U, NSTX-U will have the benefit a Li evaporator dedicated for conditioning the upper divertor. Thus, on NSTX-U, with Li conditioning of the upper divertor the CHI discharges could in principle be driven harder to allow increased absorber arcing to occur, but without the influx of significant oxygen influx.

8.3.2.3 Initially couple to induction, then assess coupling to NBI and HHFW

A good way to quickly assess the quality of discharges produced using a new start-up method is to couple it to induction using the central solenoid. Coupling to induction is a first step to assess if the confinement properties are adequate for eventual coupling to neutral beams. The goals on NSTX-U will be to initially couple to a central solenoid that has zero pre-charge, for a direct comparison to results obtained on NSTX. The extent of central solenoid flux savings flux will be measured. The electron densities and temperatures and their profiles during current ramp will be measured as a function of current ramp-rates with and without the presence of neutral beams and HHFW heating. In other experiments, some pre-charge will be introduced into the central solenoid to determine the minimum pre-charge that is needed to ramp a CHI started discharge to the 0.6-1 MA range. This would be of considerable benefit to other experiments on NSTX-U aimed at sustained non-inductive operation in the 0.6 to 1 MA range of currents as the central solenoid current could be maintained at zero after the sustainment current levels are achieved.

The next step will be to gradually reduce the loop voltage and improve the neutral beam injection parameters (based on TSC and TRANSP simulations coupled to experimental measurements) to understand the requirements for full sustainment with neutral beams during years 4 to 5. The electron temperature, especially during the first 50 ms after initiation of a CHI discharge will be particularly important for full sustainment by beams, and the 28 GHz ECH capability will not be available until Year 4 of the NSTX-U 5 year plan. In support of this goal, the temperature and density requirements of the CHI target will be studied using HHFW heating and the best-developed wall conditioning methods to increase the intrinsic CHI discharge temperature by reducing low-Z impurities to the extent possible.

8.3.2.4 Assess ramp-up of a 400 kA inductive target with NBI and HHFW

In support of Year 4-5 goals to fully ramp a 400 kA CHI target to the 1 MA levels, data will be gathered during the first two to three years in which a the CHI discharge will be experimentally simulated by using a 300-400 kA inductively generated target. In such discharges the solenoid current will be held constant and neutral beams and HHFW injected into the decaying target to determine the plasma parameters that are required for full non-inductive ramp-up. Targets with both low and high internal inductance will be used, furthermore Te will be varied to improve our understanding of the sensitivity to both current and electron temperature profiles. Changing the initial inductive current ramp rates supplemented by early heating by HHFW and NBI will generate discharges with variations in internal inductance and electron temperature. We are at present studying the NBI coupling efficiencies (using TRANSP) in these simulated targets that have been generated by TSC.

TSC simulations, such as the one shown in Figure 8.13 suggest that starting from a 400 kA inductive target, the combination of bootstrap current overdrive plus neutral beam current drive could ramp the current to 1 MA in about 3 s. In these simulations, an initial 400 kA low-inductance discharge is heated using 4 MW of HHFW power. The H-mode is initiated at 150 ms and the HHFW power is turned off at 0.9 s. The neutral beam power is programmed to increase with the plasma current. Starting from 1.5 s, a Greenwald density fraction of 0.5 and electron temperature of 1.7 keV is maintained until 5 s. The energy confinement time is maintained at about 30 ms, consistent with NSTX experimental results.

These simulations give confidence that full non-inductive current ramp-up should be possible in NSTX-U. It is also necessary to cross check the simulation results with experimental measurements to improve the model of electron transport, neutral beam absorption and current drive fractions. This would be an important part of the experimental program during Years 1 and 2 of NSTX-U operations.

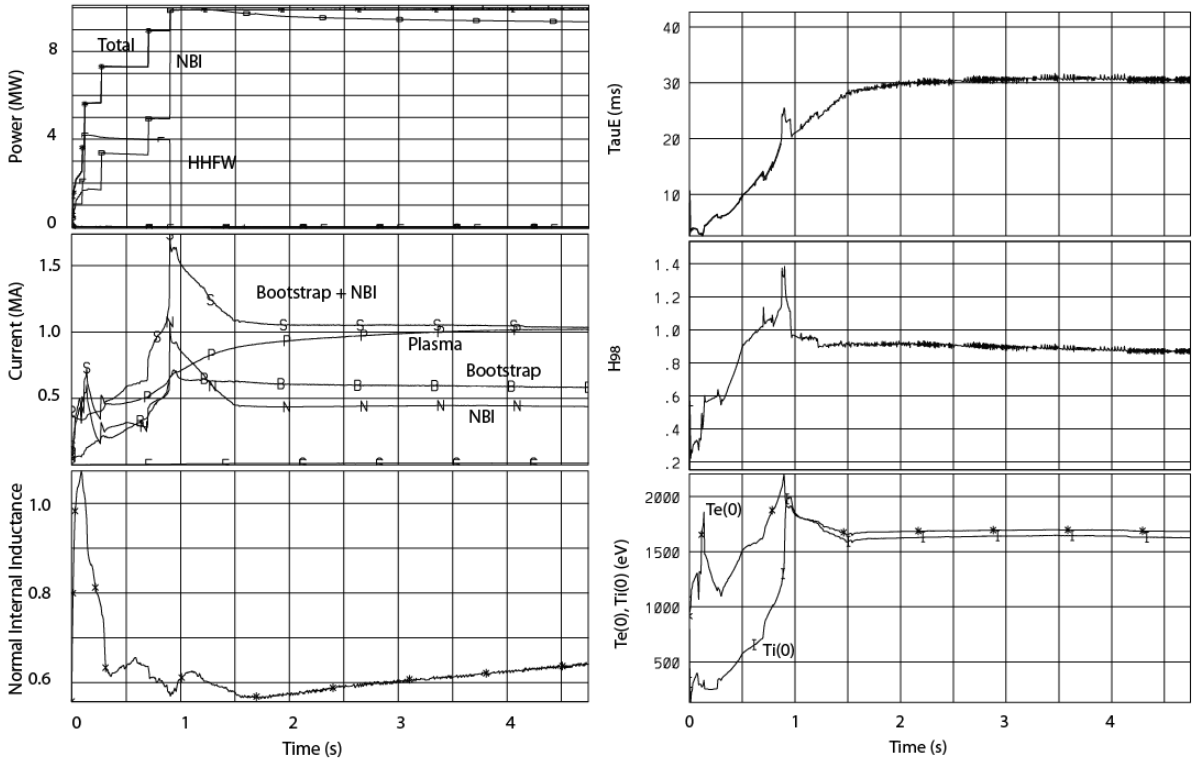

Figure 8.13: TSC simulations in which a 400 kA discharge is ramped up using bootstrap current and neutral beam current overdrive.

8.3.3 Thrust 2 Research Plans (Years 4 to 5): Ramp-up CHI Plasma discharges using NBI and HHFW and Test Plasma Gun Start-up

8.3.3.1 Establish CHI discharges using metal divertor plate electrodes

Another method to increase the electron temperature in electrode based plasma start-up methods is to use refractory metal electrodes, rather than carbon electrodes. This is because metals do not radiate strongly until the electron temperature exceeds 100 eV. Because the TCHI start-up is a pulsed method, with the electrode current driven phase lasting for less than 3 ms, any metals (even if sputtered into the discharge) should be lost in a few particle confinement times. The electrode-based spheromak experiments that generated high electron temperature plasmas (> 400 eV) used metal electrodes. During Years 4 to 5, it is planned that high-Z tiles would replace the lower divertor graphite tiles. We will run reference discharges from the Year 3 to determine the improvements to the CHI electron temperature, peak plasma current and reduction in impurities and the required CHI operating voltages that results from the use of metal electrodes.

8.3.3.2 Assess benefits and compare to QUEST results (if available)

We are currently engaged in a CHI systems design for the QUEST ST in Japan. The QUEST CHI electrode would likely use tungsten plasma spray coating on a stainless-steel substrate. In addition, QUEST will have access to a 0.5 MW ECH system. If the CHI hardware is installed on QUEST before 2015, transient TCHI results should be available from QUEST during the 2016 to 2018 time frame. These results will be compared to results obtained on NSTX-U with graphite and metal electrodes. These results from QUEST would help NSTX-U CHI research and provide additional information related to the electrode designs for a ST FNSF.

8.3.3.3 Assess benefits of lithium deposition in the upper divertor region

During the actively driven portion of a CHI discharge the E X B drift is away from the injector region and into the absorber region. As a result, over time, the neutral pressure can build up in the absorber region. This increase in gas and plasma density in the absorber region is a condition that is favorable for the generation of absorber arcs. This issue is much more pronounced during steady-state CHI during which the neutral pressure could build up to high levels. For steady-state CHI, active pumping may be required in the absorber region to keep the neutral pressure low and to deplete the region of charge carriers so as to reduce the incidence of absorber arcs. During TCHI this is much less of an issue for the following reasons. First, the neutral gas transit time is about a meter per ms. The distance between the injector and absorber regions in NSTX-U is about 4 m. So it takes approximately 4 ms for the gas injected in the injector to reach the absorber region. The actively driven CHI pulse duration is a strong function of the operating voltage. At the 1.7 kV that was used in NSTX, the active portion of the CHI pulse length was 3 ms. Thus during the 3 ms period, most of the energy from the capacitor bank is depleted before much of the injected gas reaches the absorber. So, the arcs should be mostly governed by the time taken by the leading edge of the CHI discharge to reach the absorber region. Absorber arcs generated in this manner could be suppressed through the use of a buffer flux as previously

described. Nevertheless, on these time scales some gas will get into the absorber region, and so active pumping in this region will only help. Active pumping in the absorber region may also provide more flexibility in the amount of injected gas or in the CHI operating voltage. The planned installation of an upward-pointing lithium evaporator would allow testing of the benefits of operating CHI with reduced neutral pressure in the absorber region that may result due to stronger deuterium pumping in the upper divertor region.

8.3.3.4 Maximize current start-up

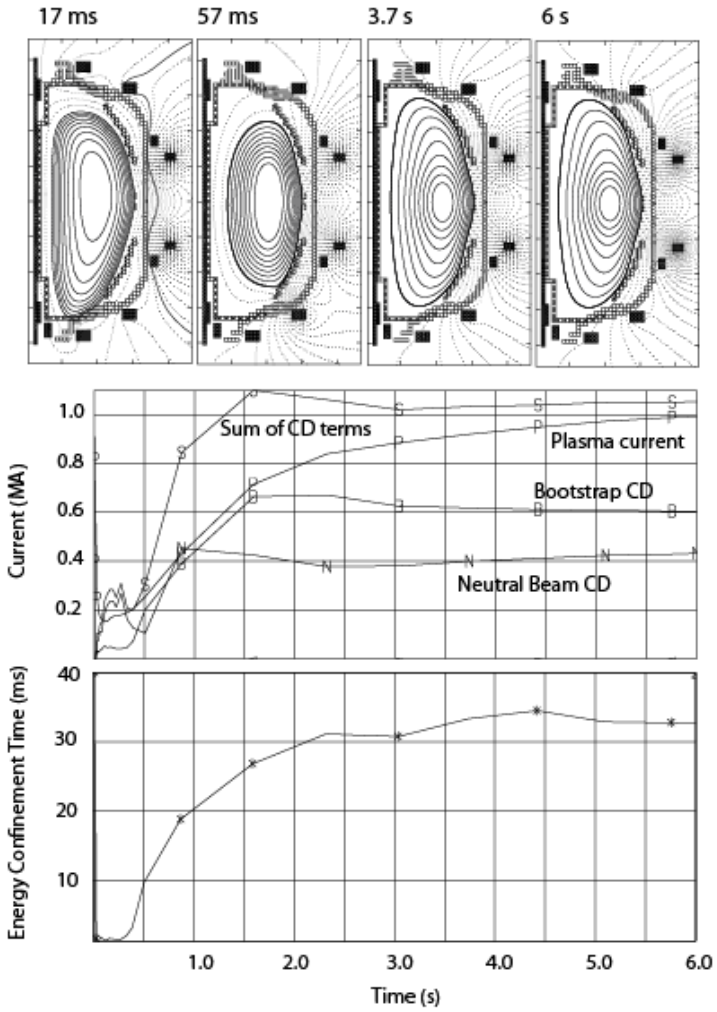

Figure 8.14: Shown are TSC results from a full discharge simulation that involves plasma start-up using CHI and current ramp-up using NBI and bootstrap current overdrive. Top frame: Shown are the poloidal flux contours at 17 ms, during the end of the CHI-phase, at 30 ms during the coupling phase and at 3 and 6 seconds during the current ramp-up phase. Middle frame: The different components of current drive. N: Neutral beam, B: Bootstrap, P: Plasma current and S: Sum of current drive terms. Bottom frame: The energy confinement time calculated with respect to input power.

During Years 2 and 3, we will have established CHI start-up and demonstrated coupling to induction. These experiments will have used graphite divertor tiles and 2 kV CHI operational capability. During Years 4 and 5 new CHI enhancing capabilities will become available. These will be used to maximize the CHI current start-up potential in NSTX-U.

First, discharges will be generated during Year 4 using metal divertor plates as described above to further reduce low-Z impurities and to increase both the electron temperature and the plasma current magnitude.

Second, higher capacitor bank voltage capability of up to 3 kV will be used to reduce the CHI pulse length and to increase the magnitude of injected poloidal flux to further increase the plasma current. To increase the injected flux at a given toroidal field, the bubble burst criterion requires that the injector current be increased. Increasing the injector current at low voltage

requires a longer injector pulse length that increases the amount of electrode generated impurities as well as increasing the possibility of absorber arcs. During TCHI, reducing the CHI pulse length during the actively driven portion is only possible by increasing the operational voltage. At the higher voltage, which would now require a bank with smaller capacitance (but more total stored energy), the higher injector currents could be achieved at shorter pulse lengths. This would both reduce the impurities injected from the injector and minimize the severity of absorber arcs. Voltage control is a very powerful knob for CHI start-up. During the FY09 and 10 CHI campaigns, NSTX-U essentially always used the maximum available voltage of 1.7 kV as a reduction to this voltage reduced CHI performance levels. This CHI voltage capability will be increased for the first time in NSTX-U, to 2 kV during Years 1 and 2 of NSTX-U operations and up to 3 kV during Years 3 and 4 of NSTX-U operations. This new capability should allow NSTX-U to use more of the available injector flux to explore the maximum levels of start-up currents possible in NSTX-U. Experimental assessment of these limits will directly influence the CHI system design for FNSF.

During this period the secondary CHI injector coil will also become operational. This would increase the CHI injector flux capability from about 220 to 340 mWb. As previously mentioned, the CHI generated plasma current scales proportional to the injector flux.

8.3.3.5 Heat CHI target using 1 MW ECH, then HHFW for coupling to NBI

TSC simulations of NSTX TCHI discharges have successfully demonstrated current persistence [33], which is the toroidal current persisting after the injector current has been reduced to zero. The generation of closed flux is the result of an effective (positive) toroidal loop voltage induced by the changing poloidal flux on the open field lines as the injector current is reduced to zero. Reference [33] also shows that CHI scaling with toroidal field is favorable for larger machines so that peak plasma currents in excess of 600 kA could be generated in NSTX-U. The higher toroidal field allows more poloidal flux to be produced in the plasma at the same level of injector current.

We have now conducted the first simulations of a fully non-inductive start-up with CHI and subsequent non-inductive current ramp-up using neutral beams in support of planned experiments on NSTX-U (Figure 8.14). The CHI discharge is initiated by TSC as described in Reference [33], and a 400 kA closed-flux target is generated. The first step involves current driven by the external injector circuit on purely open field lines. This causes the injected poloidal injector flux to fill the vessel. Then, the applied CHI voltage is rapidly reduced. This results in a rapid decrease in the injector current. As a result, the injected poloidal flux begins to reduce in magnitude. The time-changing poloidal flux induces a positive loop voltage within the plasma, which causes the generation of closed field lines carrying toroidal current.

At the onset of flux closure a second step in the simulation is initiated. This continuously solves for the plasma boundary, including locating the divertor X-point and begins solving the flux

surface averaged transport equations. This phase begins 17 ms after the CHI discharge is first initiated.

For these simulations, the initial electron temperature for the CHI discharge is 100 eV. This is a reasonable starting value based on other simulations that show that 1 MW of 28 GHz RF heating power could rapidly increase the electron temperature of a CHI-like discharge to over 100 eV. The initial electron density is assumed to be 3×10^{18} m^{-3}, similar to the densities obtained during CHI start-up in NSTX as shown in Figure 8.5. In the simulation, the initial plasma internal inductance is also below 0.5, consistent with that calculated by EFIT for the CHI discharge in NSTX shown in Figure 8.5.

At 17 ms, horizontal position control is implemented and at 40 ms vertical position control is used to vertically center the highly up/down asymmetric CHI plasma. The electron transport is adjusted to keep the energy confinement time at about 30 ms, consistent with energy confinement times in neutral beam heated NSTX discharges. During the low density phase of the discharge the RF power is increased to 2.5 MW. This is assumed to be from a combination of 0.5 MW absorbed ECH power and 2 MW of absorbed HHFW power. After that 2 MW of HHFW power is retained in these simulations. Neutral beams are added in increments to keep the current overdrive at acceptable levels, as TSC is not capable of handling the formation of current "holes" where the toroidal current density drops to zero or to very low values. After the current has built up to sufficient levels, both the density and neutral beam power are ramped-up. Figure 8.14 shows the results from this first evolving discharge, which at 6 s reaches 1 MA of plasma current.

8.3.3.6 Test plasma gun start-up on NSTX-U

During the first two years, work in progress at the Pegasus facility will focus on competing the detailed systems design for NSTX-U. During the next three-year period, the work will focus on the construction and deployment of this startup system. The complete startup system (injector hardware, control system, and power supplies) could be deployed at NSTX-U as early as Year 3 or 4. Then, initial shakedown experiments could be conducted during Year 4 or 5.

Initial experiments using the compact helicity injection system at NSTX-U will be guided by operating scenarios developed in the computational activities of the previous years, and will establish the necessary elements of a successful high-current startup. Using an active plasma source to form a tokamak-like state in the presence of the passive plates, transition of the drive from the active gun source to the passive electrode, buildup of the plasma current due to helicity injection drive, and demonstration of the plasma position control through the current buildup phase must all be experimentally demonstrated on NSTX-U before attempting a high-current startup. Optimistically, by the end of Year 5, initial experiments using the newly deployed compact helicity injection system may have demonstrated these features and the NSTX-U team may be poised to attempt a full-power 1 MA startup in the following year.

8.4 Diagnostics

8.4.1 General NSTX-U diagnostics

Standard NSTX diagnostics used for plasma operations on NSTX have been used to diagnose CHI discharges on NSTX and will continue to be used to support CHI discharges on NSTX-U. These systems are described in Chapter 10 of the 5 year plan document.

As in previous years, discharges established using CHI will be diagnosed using the multi-point Thomson scattering diagnostic to obtain electron temperature and density profiles as a function time. The multiple laser beams are triggered in close temporal proximity to each other to measure radial profiles or temperature and density during the current decay phase of a CHI discharge. The far infrared tangential interferometer/polarimeter (FIReTIP), will be used in conjunction with the Thomson scattering diagnostic to provide continuous line-integrated density measurements.

Visible and VUV spectroscopy will be used during control room operations to improve discharges so as to minimize the influx of low-Z impurities. These have been quite helpful in the past for assessing vessel impurity levels and for qualitatively assessing impurity levels in CHI discharges.

The fast camera diagnostic has also been very effective for quickly determining the shape of the evolving discharge and for controlling the discharge during the pre-programmed coil current phase. The Plasma TV system provides a fisheye view of the entire NSTX plasma from a re-entrant port located on Bay B midplane. A Vision Research Miro 2 color camera is used. The camera has a 10 bit depth and has a full frame acquisition speed of 1.24 k frames per second (fps) @ 640x480 pixels. The resolution typically used varies between 448x448 pixels and 176x176 pixels (the latter being more commonly used in CHI experiments). These resolutions correspond respectively to a maximum frame rate of 1.8 kfps and 10 kfps. Qualitative information about the radiating species can be obtained from the color of the emission. Two wide-angle lower divertor views (Bay E and Bay J) will be available in the same configuration as in 2010, providing a full toroidal coverage of the lower divertor [34]. In the 2010 configuration a Vision Research Phantom 7.3 and a Vision Research Phantom 710 were used with 12 and 14 bit depth resolutions. The Phantom 7.3 has a maximum full frame acquisition speed of 6.8 kfps (800x600 pixels) while the Phantom 710 has a maximum full frame acquisition speed of 7.5 kfps (1280x800 pixels). The typical resolutions are of 256x208 pixels (Phantom 710) and 224 x 184 (Phantom 7.3), which correspond to maximum acquisition speeds of respectively 100 kHz and 60 kHz and resolutions of about 0.8 cm/pixel. Reducing the field of view acquisition speeds up to 200 kHz were achieved in the same configuration. These cameras are equipped with remotely controlled filter wheels.

The multi-energy SXR array with, eventually, two toroidally displaced sets of views has a frequency response <100 kHz. Spatial resolution varies from ~1 cm at the outboard midplane

(130<R<150 cm) to ~3 cm in the core region (90<R<140 cm). Faster measurements with up to ~500 kHz bandwidth will be available from a system of two poloidal SXR arrays. Each array contains 16 channels viewing poloidally through two variably selected filters, with 2-3 cm resolution. The system can also be operated in the bolometer mode to obtain total radiated power profiles. Additional descriptions of these systems are provided in Chapter 10.

New for NSTX-U will be a Motional Stark Effect with Laser-Induced Fluorescence (MSE-LIF) diagnostic. Comparing to the MSE diagnostic on NSTX, MSE-LIF does not rely on heating beams and has its own dedicated diagnostic neutral beam with beam energy of 30-40 keV. Different from conventional MSE, which depends on emission from collisionally induced fluorescence, MSE-LIF uses laser to induce fluorescence and thus leads to stronger emission. Beam voltage is swept across spectrum and spectral peak separations can be measured, from which magnetic field magnitude can be obtained, and additional polarization measurement provides pitch angle information. Preliminary measurements from beam-into-gas shots on NSTX show a sensitivity of 5-10 gauss for the field amplitude measurement. MSE LIF will be used to measure the magnetic field line pitch angle, which will be used to measure q profile in CHI discharges. The time response of the system is 10 ms, which should be sufficient for longer pulse, higher-current CHI start-up discharges expected in NSTX-U. The spatial resolution is 2-3 cm. These measurements will be used to further improve CHI start-up simulation capability using the NIMROD and TSC codes.

8.4.2 CHI specific diagnostics

CHI Voltage monitors: During CHI operations, the voltage of the inner and outer vessel with respect to ground is individually measured. On NSTX, the voltage was measured using a resistive-divider network that was connected to the vessel near the bottom of the machine (near the injector region). The electrical signals were then converted to optical signals using a fast fiber optic transmitter/receiver system and then recorded on a remote digitizer known as a handyscope. The handyscope was floated with respect to NSTX ground. Because much of the long-distance signal transmission was over a fiber optic network, the system avoided electrical noise pick-up including ground loops and so had a high system bandwidth of more than 100 kHz and was digitized at sample rates of 1 MHz. For NSTX-U, this system will be retained and an additional duplicate system installed to measure the voltage on the upper part of the vessel as well. In addition to these we will digitize the signal from a separate voltage divider network without the use of a fiber optic network using conventional digitizers. This back-up system will be functional for all NSTX-U discharges and will have a much slower bandwidth of 10 kHz.

CHI current monitors: The CHI injector current is measured at the CHI capacitor bank location using a Pearson current transducer mounted on the CHI current feed to the vessel. This system will be retained for NSTX-U operations. In addition, we plan to install additional current transducers near the CHI connections to the NSTX-U vessel. There will be a total of four

additional current sensors composed of a Pearson current transducer and a Direct Current Current Transducer (DCCT) on each of the input and return current legs to the machine. These would be located on the machine side of what is known as the McBride switch. The McBride switch functions to either short the inner and outer vessel components or allow them to be individually biasable. The purpose of the new current monitors would be to further improve the resolution of the current measurements during CHI as well as to provide current measurements across the vessel components during normal NSTX-U operations to measure divertor halo currents and thermoelectric currents during standard inductive operation.

New set of inner vessel magnetics: During NSTX CHI operations, especially during discharges in which a long pulse edge current was driven using the CHI DC power supplies, it was observed that the inner vessel magnetics were prone to EMI noise pickup. This was largely due to inadequate shielding of the sensors mounted inside the inner vessel casing. For NSTX-U we will have an array of sensors that will be specially shielded for EMI using a braid that fully surrounds the return current leads. Because of space limitations inside the center stack casing this was not possible on NSTX. For NSTX-U, the number of such specially shielded sensors is reduced to provide adequate space for the braid inside the center stack casing.

Additional flux loops and Mirnov coils on lower and upper divertor: To improve the measurement of the CHI injector flux and in support of NIMROD simulations, two additional Mirnov coils and an additional polodal flux loop will be added to each of the upper and lower divertor plates on NSTX-U.

Electrode diagnostics: NSTX-U will have a Langmuir probe array at one toroidal location on the lower outer divertor plate. The sensors will provide information on the radial changes to the ion saturation current and the floating potential and will be useful for localizing the region where the CHI injector current flows. In addition to these sensors, a dual color, fast infrared camera will be used to measure the plate temperature during CHI operations. A third diagnostic is a fast visible camera that can be used either as a visible camera or as a filtered camera to view light emissions from lithium or carbon lines. All three of these diagnostics will be used to determine the radial extent of the CHI injector current. This information will be used to improve simulations using the NIMROD code.

8.5 Theory and Simulation capabilities

8.5.1 2D equilibrium evolution simulations

TSC is a time-dependent, free-boundary, predictive equilibrium and transport code [35 36]. It has previously been used for development of both discharge scenarios and plasma control systems. It solves fully dynamic MHD/Maxwell’s equations coupled to transport and circuit equations. The device hardware, coil and electrical power supply characteristics are provided as input. It models the evolution of free-boundary axisymmetric toroidal plasma on the resistive and energy

confinement time scales. The plasma equilibrium and field evolution equations are solved on a two-dimensional Cartesian grid. Boundary conditions between plasma/vacuum/conductors are based on poloidal flux and tangential electric field being continuous across interfaces. The circuit equations are solved for all the poloidal field coil systems with the effects of induced currents in passive conductors included. Currents flowing in the plasma on open field lines are included, and the toroidally symmetric part of this "halo current" is computed. For modeling CHI in NSTX, the vacuum vessel is specified as a conducting structure with poloidal breaks at the top and bottom across which an electric potential difference is applied from which TSC calculates the injector current using a model for the resistivity of the "halo" plasma. This circuit, however, contains a sheath resistance at each electrode, which is difficult to model.

Shown in Figure 8.15 is the simulation of an early NSTX TCHI discharge that successfully demonstrated current persistence, a condition when the CHI produced toroidal current persisted after the injector current had been reduced to zero. We used the same poloidal field (PF) coil currents as were used in NSTX Shot 118340 [5]. Due to the difficulty in computing the actual plasma resistance including the plasma-vessel sheath resistance in this case, we did not attempt to use the experimentally measured voltage, but rather applied a voltage V across the lower vessel gap and adjusted this value V to give approximate agreement with the measured toroidal current. About 60 kA of toroidal current is generated soon after the current peak, and as in the experiment, at the time of peak toroidal current, the injector current is similar to the experimental value. The poloidal flux plots show the plasma evolves in much the same way as observed experimentally from fast camera images.

In these simulations the injector voltage is varied by a controller to obtain the required injector current. This is similar to what is done experimentally. The injector current is the parameter that needs to be controlled. For example, experimentally, for identical injector flux conditions in the same machine a different value of the voltage may be required to produce the same injector current since the magnitude of the injector current depends on the resistivity of the plasma and the edge sheath conditions. These depend on many things that are difficult to predict such as the conditioning of the machine, the presence of impurities, and the possible presence of auxiliary heating. Experimentally, if we are unable to get the injector current needed to inject a given amount of poloidal injector flux, then we simply increase the voltage to a level that is required to obtain the needed injector current.

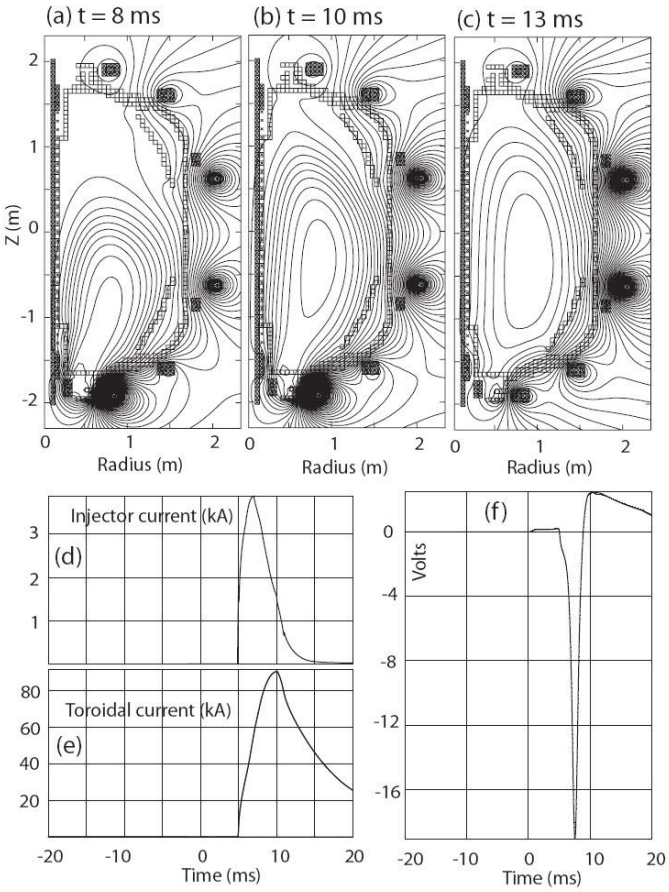

Figure 8.15: Simulation of a 60 kA NSTX TCHI discharge (shown in Reference 33) with the TSC code. For these simulations, the coil currents used in the experiment were used as input parameters. The CHI voltage is applied at 5 ms. Shown are (a-c) poloidal flux contours, (d) the injector current, (e) the plasma current and (f) the induced loop voltage at Z = -0.3 m along the inner vessel during the growth and decay of the CHI plasma discharge.

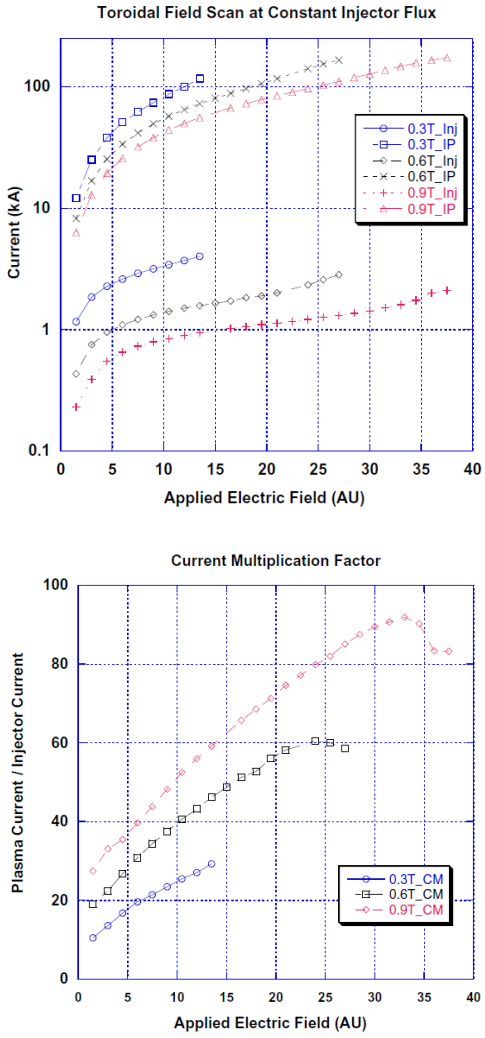

Figure 8.16: The top frame shows the injector current (lower traces) and the CHI produced toroidal current (top traces) as the injector voltage is increased. The lower frame is the ratio of the toroidal current to the injector current and represents the attained current multiplication factor.

Generation of closed flux in TSC is as a result of an effective toroidal loop voltage induced by the CHI ejected poloidal flux that decreases as the injector current is reduced to zero, as shown in Figure 8.15f. These are described in more detail in Reference [33].

Shown in Figure 8.16 is the result of several TSC runs in which the injector flux was maintained constant and the toroidal field was increased. Simulations were run at 0.3, 0.6 and 0.9 T. For each of these cases the applied electric field across the CHI injector gap was sequentially increased until the discharge filled the vessel and began to interact with the absorber region. In the upper plot shown in Figure 8.16, the three lower traces correspond to the injector current and the three upper traces correspond to the CHI produced toroidal current. The injector current

shows an initial change in slope as the voltage is increased. The inflexion point of this trace is related to the bubble burst current. Thus as the toroidal field is increased, less injector current is required to satisfy the bubble burst current while a higher voltage is needed to get to same injector current as for the lower toroidal field case. This indicates that at 1 T, a slightly higher voltage capability may be required on NSTX-U, but probably less than a factor of 2. Additional analysis is needed to establish the voltage requirements for NSTX-U.

The lower frame of Figure 8.16 shows the attained current multiplication for the three toroidal field cases and it shows the multiplication to significantly increase with toroidal field. The maximum current multiplication seen in these discharges is similar to the values achieved experimentally, which varies from 60 to nearly 100 for some discharges. These results for the simulations, are consistent with the earlier simple model developed by Jarboe [27], which states that the minimum injector current to meet the bubble burst condition is given as, $I_{inj} = 2\Psi_{inj}^2/(\mu_0^2 d^2 I_{TF})$ where I_{TF} is the current in the toroidal field coil and d is the width of injector flux "footprint" on the electrodes.

Given the resolution of the data points near the inflection point, the inflection point for the 0.9 T case occurs at about 0.65 kA, around 0.95 kA for the 0.6 T case and around 1.85 kA for the 0.3 T case. Because the injector flux magnitude and the flux footprint width are not varied in these simulations, the $1/B_T$ scaling is seen in these TSC simulations. It is seen that the discharge with the highest value of toroidal field does indeed require less injector current. As the toroidal field is increased, the injector impedance increases. This is a consequence of the longer field line length, which now requires more voltage to drive a similar magnitude current. Thus for these three cases, as the toroidal field is increased, the injector voltage also needs to be increased to be able to drive an adequate amount of injector current.

Results from Ref. [27] also show that the attained current multiplication factor should vary as the ratio of the toroidal flux in the vessel to the injected poloidal flux (the gun flux). This trend is also seen in the TSC simulations. An examination of the highest current multiplication factor attained for the three toroidal field cases shows that after the discharge fully fills the vessel, a condition that is reached at close to the highest value of the applied electric field for each of the cases, the 0.3 T case has a current multiplication factor of about 29, it is 59 for the 0.6 T case and 90 for the 0.9 T case, again reflecting the effect of the toroidal field scaling. Thus, machines that have a higher toroidal field or a larger physical plasma volume would have higher values of the current multiplication factor in achieving a given plasmas current. The higher multiplication with size has also been observed experimentally. The smaller HIT-II machine typically saw current multiplication factors of 6, whereas NSTX, which has ten times more toroidal flux than HIT-II typically, sees a current multiplication factor of about 60.

Plans for TSC simulations: The non-inductive plasma start-up and current ramp-up program on NSTX-U will make extensive use of TSC simulations coupled to TRANSP/NUBEAM and RF codes (such as GENRAY) to adequately understand non-inductive current ramp-up requirements for NSTX-U and an ST FNSF. TSC will be used to simulate the scenario and will provide experimental-like conditions to TRANSP/NUBEAM, which will be used to calculate the heating a nd current drive profiles that are given back to TSC for re-calculation of the scenario. Alternatively, the SWIM framework will also be used, with TSC calling directly NUBEAM and GENRAY. An example of a TRANSP simulation for a 300 kA plasma discharge in NSTX is shown in Figure 8.17. On NSTX-U there are a total of 6 individual beam sources, each at a different tangency radius. The absorbed and loss power in MW for the traces in Figure 8.17 are for an injection power of 2 MW for each source. The simulations are for each individual source at injection energy of 65 or 80 keV.

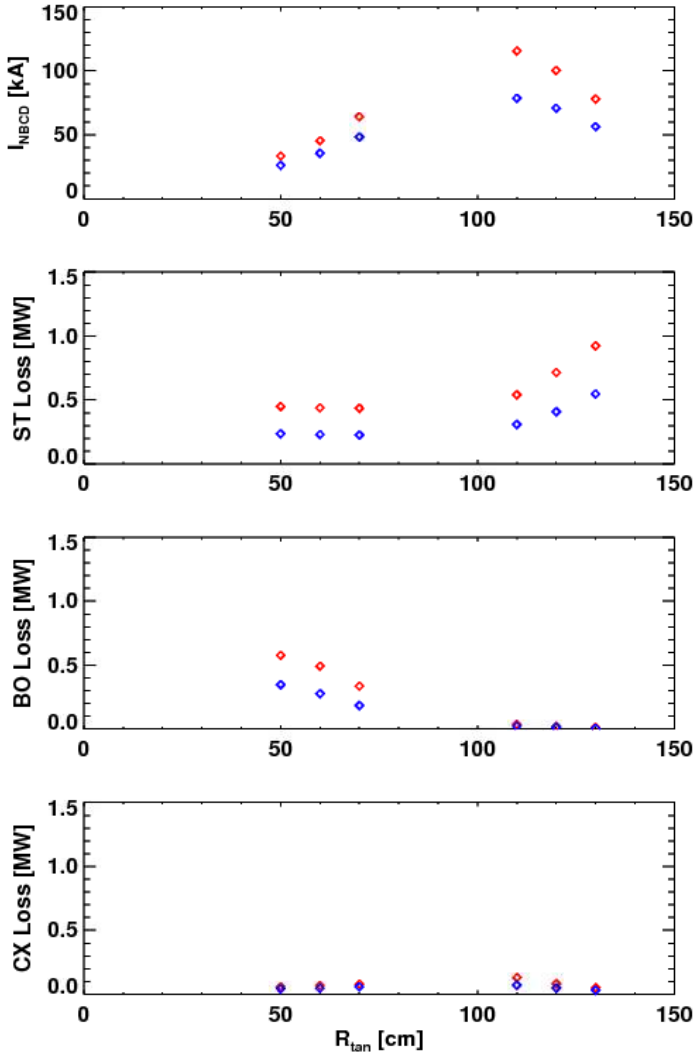

Figure 8.17: TRANSP simulations of NBI coupling efficiency for a 300 kA discharge at a density of ~1.3E19 /m^3. Red is for 80 keV NBI energy and blue is for 65 keV injection energy. The power each source is 2MW. Shown from top to bottom are the NB driven current, the shine through loss, the bad orbit loss and charge exchange loss power all as function of beam tangency radius.

Figure 8.17 shows that the absorbed current drive efficiency increases from about 40 kA to about 120 kA, a factor of 3 increase, as the tangency radius is increased from that of the least tangential source (RTAN = 50 cm) of the present NBI with the least tangential radius (RTAN = 110 cm) of the new 2nd NBI. Even for the new sources at 120 and 130 cm the NB current drive efficiency is significantly higher than for the present sources that have a tangency radius of 70 cm or less. The NBI power loss is also a function of tangency radius, and Figure 8.17 shows that for small RTAN, the more perpendicular injection increases the number of particles that are promptly lost (i.e. bad orbits).

Figure 8.17 also shows that large R_{TAN} can lead to increased power losses due to increased shine-through. This is caused by the decrease in NBI path-length intersecting the plasma when RTAN is large, and this results in decreased beam ionization and absorption. However, for the source with a tangency radius of 110 cm, it is about the same as that for the present NBI sources. The charge exchange losses for all sources are small. Overall, the current drive efficiency for injected power is at least 50-100% higher for the new 2nd NBI compared to the present NBI.

Before the start of NSTX-U operations we will have developed a TSC geometry of the NSTX-U vessel and used it to simulate initial CHI plasma start-up. These early simulations are needed for planning the initial CHI start-up experiments to be conducted during Year 1 of NSTX-U operations. TSC will be used to assess the favorable B_T and injector flux scalings indicated by the NSTX CHI experiments and by NSTX TSC simulations. These will be compared to and improved after CHI discharges are established and improved during Years 1 and 2 of NSTX-U operations.

Starting from 2013 and extending into Years 1 and 2 of NSTX-U operations, we will use TSC coupled to TRANSP/NUBEAM and RF codes to adequately understand the initial seed plasma parameter requirements for current ramp-up to the full 1 MA sustainment levels planned for in NSTX-U. Of particular interest are the importance of Z_{eff}, electron density levels and ramp rates, electron temperature and density profiles, the transport models used, electron and ion thermal diffusivities and the plasma shape. Much of this work will be carried out in parallel with experiments on NSTX-U so that a realistic TSC/TRANSP model of non-inductive current ramp-up will be developed. To develop this model, we will initially rely on TRANSP/NUBEAM simulations of representative discharges that have profiles and plasma parameters similar to the type of discharges developed on NSTX, but also extending the range of parameters to adequately cover the CHI target parameters anticipated in NSTX-U.

During Years 2 to 4 the TSC model being developed for inductive discharges will be used to model neutral beam coupling to CHI discharges that would now be available.

During Years 4 and 5 we will adapt the TSC models that have been validated with NSTX-U experimental results to simulate non-inductive current start-up and non-inductive current ramp-up in a ST FNSF device. We will also begin to implement the CHI start-up scenarios directly in TRANSP, after the TRANSP free-boundary predictive capability matures to a level where its use becomes routine for NSTX-U inductively generated discharges.

8.5.2 3D resistive MHD simulations – NIMROD, M3D

The present understanding of transient CHI start-up implies that much of the scaling and projections to larger machines could be carried out using 2D simulations with the TSC code. The primary goal of NIMROD simulations is to understand the impact and role of any possible 3D physics mechanisms in transient CHI plasma formation. NIMROD studies will investigate the

role of additional 3D physics to see if the 2D calculation is valid, especially as the plasma current is increased. The primary parameters of interest are the injector and plasma current ramp-up time histories, effect of voltage programming, the poloidal flux evolution and the electron temperature and current profiles during the initial 1 to 10 ms of the plasma formation phase.

The NIMROD code (Non-Ideal Magnetohydrodynamics with Rotation, http://nimrodteam.org) solves linear and nonlinear plasma models including magnetohydrodynamics, two-fluid systems, and kinetic extensions as 2D and 3D initial-value problems. The spatial representation features a 2D plane of nodal spectral finite elements for geometric flexibility and accuracy in the extremely anisotropic conditions that characterize magnetized plasmas, [37] and the third direction is assumed to be periodic (cylindrical/toroidal or straight) and uses the finite Fourier series spectral method. The temporal advance staggers flow velocity from other fields. Implicit methods are used when advancing the physical fields in time to avoid numerical stability limits that are associated with wave and flow propagation in the multiscale problems of interest. [38] Kinetic extensions include a simulation-particle-based method for drift and large-orbit effects from a minority species of hot ions. [39] In addition, important nonlocal effects from free-streaming particles are modeled with integral closures that evaluate the drift-kinetic equation for parallel heat flow and stress. [40]

The goals with 3D resistive MHD simulations are two fold. First is to better understand the CHI dynamics during the initial 3 to 10 ms of a CHI discharge and second to model neutral beam coupling and current drive in CHI generated plasmas.

The initial objective is to produce large volume open flux that fills the entire vessel and then test flux closure. Turning off the injector voltage to determine conditions under which closed flux is generated will test flux closure. Initially these simulations may be conducted using pre-programmed coil currents; Then, by using coil currents from a NSTX experimental discharge. Vessel eddy currents may be ignored during these initial runs. After this, we will include the vessel eddy current effects by using the time changing boundary flux generated by the LRDFIT code.

Beyond this, other physics capabilities will be added to determine limiting factors, i.e. the impact of adding electron temperature and density evolution. Simulations at this stage, that correctly reproduce the primary parameters noted above, should be suitable for studying the effects of adding n=1 and higher order modes. We will now vary parameters and understand mechanisms that lead to closed flux generation and control parameters that maximize closed flux generation. These are: Injector gap width, injector current ramp rates, voltage programming history, changes to required voltage for static and time varying injector flux, resistivity of the plasma in the injector, resistivity of the bulk CHI plasma (based on Te ~ 10eV, 20eV, 50eV, 100eV), bulk CHI plasma density and the effect of oxygen impurities in the discharge.

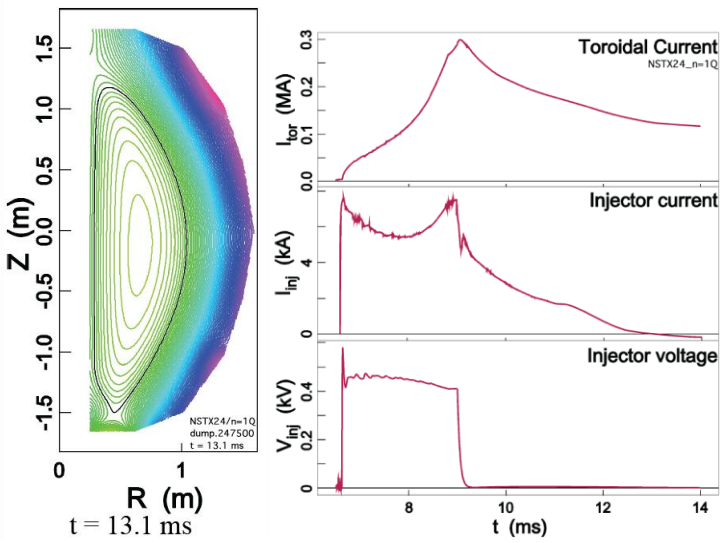

Figure 8.18: Flux surface closure for a simulation of a 4-cm wide injection slot. (a) "Fast" closure within 50 μs after rapidly reducing the injection voltage. The flux plot is for t = 13.1 ms (b) Injector voltage and current; Toroidal current for (a).

Part way through these studies, the code would be modified to study NBI coupling to CHI generated targets to understand the required CHI parameters and NBI parameters that improve NBI current drive.

Resistive MHD simulations using the NIMROD code are at present being used to model CHI start-up in NSTX; to improve understanding of the physics of injection, flux-surface closure, and current drive for CHI plasmas; and to extend these results to NSTX-U. During FY12/13 the NSTX model was improved by comparison with experiment and exploration of simulation parameters. Flux surface closure following the helicity-injection pulse has been observed in recent simulations, as shown in Figure 8.18, and is being understood. Critical to the closure has been a narrow 4-cm wide injection slot as used in the experiment and a rapid, monotonic voltage reduction at the end of injection. An X-point forms above the injection slot resulting in a separatrix surrounding a closed flux region. These results were obtained in an axisymmetric simulation indicating that resistive effects are important. A narrow current foot-print along the bottom boundary of NSTX (due to the narrow injection slot) may be needed for the reconnection generating this closure. The enclosed volume and toroidal current decay slowly following closure, although faster than experimental results. Ongoing, near-term research is directed to obtaining a larger volume of closed surfaces, to demonstrating improved quantitative comparison with experiment, and to determine the optimum conditions for closure.

Neutral-beam current drive is planned for building significant plasma starting from a NSTX-U start-up plasma generated by CHI. Nimrod will be used to simulate neutral-beam injection in NSTX-U.

Because NIMROD evolves time-dependent equations for the spatial distributions of number density, flow velocity, temperature, and magnetic field, effects of neutral beams in NSTX-U will be modeled as source densities in these equations. Source densities have been used in other NIMROD applications. For example, Ref. [41] describes resistive-MHD modeling which includes effects from ECCD that is targeted to reduce magnetic islands in tokamaks. The magnetic-field evolution in these simulations includes an effective electric-field source density in Ohm's law that represents an average force density from the RF on the electrons. This source

density is spatially localized in the poloidal plane and has nonzero curl to induce magnetic field and current density. In these simulations, the source density represents the RF effects in an ad hoc manner. More recent work by Jenkins [41] also couples wave propagation and deposition that are based on the wave electric field and quasilinear diffusion coefficient computed by the GENRAY code. The source density in these integrated simulations is localized toroidally and poloidally. Modeling of DC current injection from miniature plasma guns in the Pegasus ST uses similar source densities in NIMROD simulations. Results described in Ref. [42] have been computed with a source density in the magnetic-field equation and a source density in the temperature evolution to model the heat supplied by the plasma guns. Here, the source densities are spatially localized in the poloidal and toroidal directions.

Incorporating the effects of neutral beams in startup transients in NSTX-U can be addressed similarly to the ECCD and current injection modeling described above. Local source densities based on transport computations can be included in the advances to magnetic field, temperature, and momentum density. Each may be handled in one of two ways that are analogous to constant voltage and constant current sources in electrical circuits. Simply specifying a source-density magnitude adds energy, but the time-asymptotic effect will depend on transport. As an alternative, one may specify the source as a target value and a relaxation rate. A momentum source density, for example, would be $mn\nu(\mathbf{x})(\mathbf{V}_b - \mathbf{V})$ in this approach, where $\nu(x)$ is a relaxation-rate function that is local to the beam deposition region, V is the flow velocity, and V_b is the specified asymptotic flow-velocity. Note that this second form can act as a sink if other dynamics tend to accelerate flow in the direction of the applied force density.

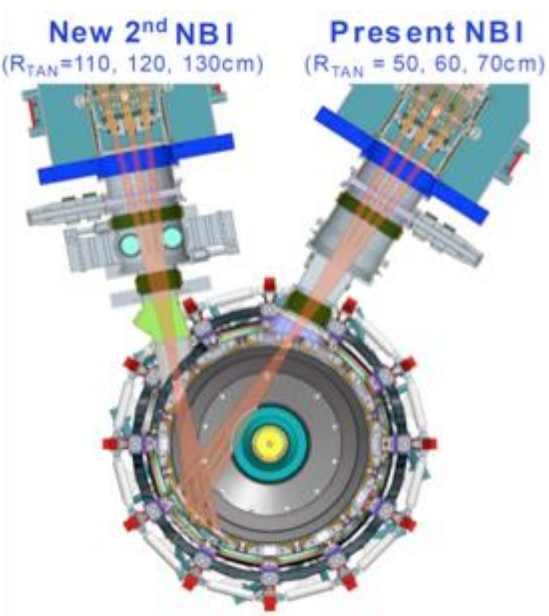

Figure 8.19. Neutral beam injection into NSTX-U. The total power available from the two beams will be 10 MW at 80 kV, 5s to 14 MW at 95 keV. Each beam system has three individual sources at different tangency radius.

NSTX-U will have two neutral beams with energy of 65-95keV. The beam geometry is shown in Figure 8.19. TRANSP calculations have shown that the second more tangential beam is well suited for driving current and will be the primary system (in addition to bootstrap current drive) for ramping the current generated by a CHI target. In support of incorporating the neutral beam model for NSTX-U CHI discharge within NIMROD, we plan to initially use standard inductive discharge parameters from NSTX discharges and then to arbitrarily vary the electron density, electron temperature and plasma current in these simulated plasmas and to compare the Nimrod results to those obtained from TRANSP simulations. After

satisfactory agreement between both codes we will switch to using the NIMROD NBI model on simulated NSTX-U CHI discharges.

The M3D-C code [43, 44] represents a complete rewrite of the older M3D 3D MHD code. It can be run as resistive MHD or two-fluid MHD, and also can be run as either 2-variable or 4-variable reduced MHD. The code is fully implicit using the split-implicit method and this enables it to take large time steps and run to long time. It uses high-order finite elements in 3 dimensions. These elements force the function and its first derivative to be continuous. This property allows spatial derivatives up to 4th order to be treated when using the Galerkin method. This property is essential for an implicit formulation using the potential/stream function form of the velocity field and magnetic vector potential. Initially we will rely on the NIMROD code for much of the 3D CHI simulations but will also consider using M3D based on future needs.

8.5.3 GENRAY-ADJ for EC/EBW Heating and Current Drive

The GENRAY [45] ray tracing numerical code, and the ADJ [46] Fokker-Planck numerical simulation are used to model electron cyclotron (EC) and electron Bernstein wave (EBW) heating and current drive during plasma start-up and plasma current ramp-up. An example of GENRAY-ADJ simulation results for second harmonic 28 GHz X-mode EC heating in a NSTX CHI start-up plasma with an axial toroidal field, $B_T(0)$ = 0.5 T (shot 148072) is presented below. Figure 8.20(a) shows the electron density and temperature profiles that were used for the GENRAY-ADJ modeling. As shown in Figure 8.20(b), 28 GHz microwave power is resonant with the second harmonic EC resonance ($2f_{ce}$) at a major radius (R) of 0.9 m. The right hand cutoff (f_R) is just below 28 GHz at R = 0.9 m.

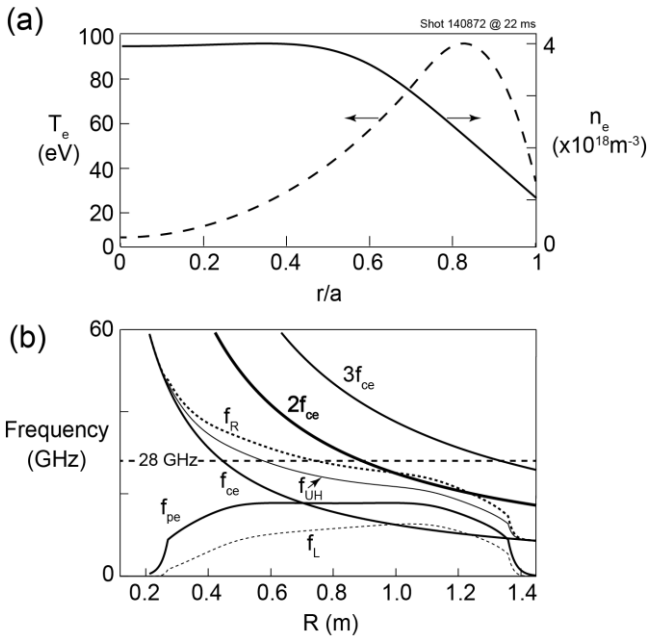

Figure 8.20(a) Electron density (solid line) and temperature (dashed line) profiles used for the GENRAY-ADJ ECH modeling, derived from multi-point Thomson scattering data acquired at 20 ms during NSTX CHI shot 148072. (b) Electron cyclotron resonances and cutoffs on the midplane of shot 148072 calculated using magnetic equilibrium data at 22 ms and the density profile data of Figure 8.18(a).

In a series of simulations the EC antenna orientation was adjusted for maximum first pass absorption. Figure 8.21 shows the ray trajectories calculated by GENRAY when the antenna was oriented for maximum first pass absorption. The power deposition profile is relatively narrow and located

at a normalized minor radius, r/a ~ 0.17 on the low field side of the magnetic axis (Figure 8.21(c)).

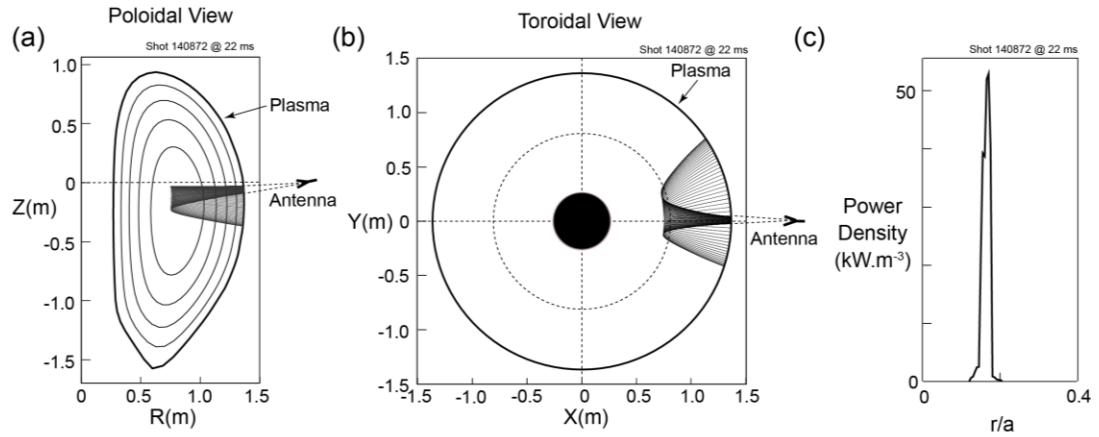

Figure 8.21: Ray trajectories calculated by GENRAY plotted in (a) the poloidal and (b) the toroidal midplane for the case with maximum first pass absorption of 28 GHz ECRH at 20 ms during NSTX CHI shot 148072, with the antenna pointing 5 degrees down and 1 degree right of the normal to the ECRH port. (c) First pass power deposition profile versus normalized minor radius (r/a) calculated by GENRAY for 1 MW of 28 GHz.

Figure 8.22(a) shows the dependence of the first pass absorption on toroidal launch angle. The peak first pass absorption reaches 27% with the antenna pointing 1 degree from normal to the plasma surface, and falls to 10-15% as the toroidal angle is increased from 3 to 8 degrees. The

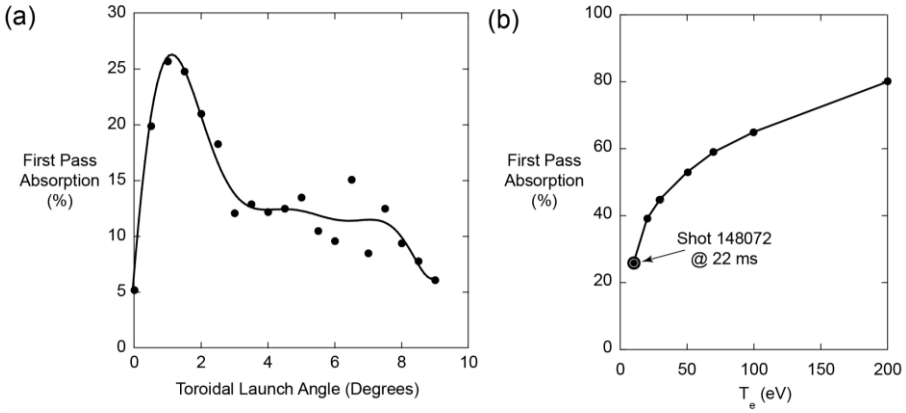

Figure 8.22: (a) First pass absorption fraction plotted versus the toroidal angle between the antenna axis and the normal to the plasma surface when the antenna is pointing 5 degrees down, and (b) the dependence of first pass absorption on electron temperature when the antenna is pointing with a toroidal angle of 1 degree to the normal to the plasma surface and 5 degrees down.

actual absorption will probably be enhanced significantly by wall reflections. As the core electron temperature rises as a result of the EC heating the first pass absorption increases, reaching about 60-80% when the central temperature is 100-200 eV (Fig 8.22(b)).

GENRAY simulation results shown in Figs. 8.21 and 8.22 were produced by launching the rays at the last closed flux surface rather than from the EC antenna. GENRAY has been upgraded to include a scrap-off layer (SOL) model and edge fluctuations. This will be particularly important for modelling EBW heating. More details of the SOL and fluctuation upgrade to GENRAY are presented in section 7.3.1.3 of the 5-year plan.

8.6 Summary

An important objective of NSTX-U is to demonstrate full non-inductive start-up and ramp-up using at least one non-inductively generated seed plasma. A second parallel objective is to understand current-ramp physics and the requirements for current ramp-up in a ST-FNSF. At present, CHI research on NSTX has made sufficient progress to provide confidence that, with the new capabilities available on NSTX-U, CHI targets could achieve this objective within the present 5 year time frame. EBW and Plasma gun generated targets will also be used as they become available. In support of these important goals, during the first two to three years, we will be conducting NBI plus bootstrap current overdrive ramp-up studies on inductively generated targets that have varying current and temperature profiles. Experimental results obtained from these studies, and later with ramp-up of CHI initiated plasmas, will be compared to TSC/TRANSP simulations to improve our models for current ramp-up requirements for an ST-FNSF. This work is also of considerable importance to AT plasma operation in tokamaks.

CHI research on NSTX-U will benefit from numerous new upgrades that are needed for a demonstration of full non-inductive current start-up and non-inductive current ramp-up to the 1 MA current sustainment levels. These are (1) higher toroidal field, (2) higher injector flux, (3) improved absorber coils, (4) ECH system, (5) tangential neutral beam system, (6) improved Li coating coverage, (7) higher CHI voltage capability, and (8) metallic divertor plates. These are briefly described below. These upgrades to NSTX-U are described in Chapter 10. Chapter 10.5.3 specifically discusses upgrades related to Start-up and Ramp-up.

Higher toroidal field: As previously discussed, the current multiplication factor in CHI discharges increases with the magnitude of the toroidal field. This means that for a doubling of the toroidal flux twice as much injector flux can be injected at the same value of the injector current. The toroidal field in NSTX-U will be 1 T, approximately twice that in NSTX. This in combination with the other upgrades described below will allow NSTX-U to generate much higher (more than 2x) levels of plasma current than what was possible on NSTX.

Higher injector flux: In TCHI discharges, the magnitude of the CHI generated plasma current is directly proportional to the injected poloidal flux. As previously noted (Figure 8.8), improved positioning of the divertor coils on NSTX-U allows the injector flux in NSTX-U to increase to 220-340 mWb. This is an increase of 2.75 to 4.25 times that in NSTX. On NSTX using 40 mWb of injector flux 200 kA of closed flux current was generated. Thus NSTX-U has very high

injector flux capability. With improved divertor plates and higher CHI voltage capability, NSTX-U in principle has the capability to generate all of the current needed at the 100% non-inductive sustainment levels (see Table 1). The initial goals, however, are to modestly double the closed flux current achieved on NSTX, which should be much easier to accomplish.

Improved absorber coils: As the CHI discharge grows in elongation, it can contact the upper divertor and bridge the upper divertor gap generating a condition known as an absorber arc. NSTX relied on two specially installed coils in the upper divertor region. Known as absorber flux coils, these generate a buffer magnetic flux in the upper divertor region that transiently delay the contact of the CHI plasma with the upper divertor until the CHI capacitor bank voltage has dropped to a sufficiently low level, so that even in the event of plasma contact an absorber arc could not be generated or it would be sufficient weak to have any detrimental effect on the CHI discharges. On NSTX-U, because of improved positioning of the upper divertor coils, (Figure 8.8) it is not only better positioned than the dedicated absorber coils on NSTX, but also has more than twice the current slew rates of the coils used on NSTX. These coils should therefore be more effective for absorber arc control.

ECH system: As previously described, direct coupling of a CHI discharge to current drive using NBI requires a plasma temperature on the order of several hindered eV. To meet this need an electron cyclotron heating system is most suited. The CHI plasma electron density is below the cut-off density for 28 GHz ECH propagation. The details of the proposed ECH system are described in Chapters 7 and 10.4.2.

Tangential Neutral Beam System: As previously discussed, a major objective of NSTX-U is the demonstration of full non-inductive current start-up and current ramp-up. This will be achieved primarily using the second more tangential neutral beam that NSTX-U will have. This system is described in Chapter 10.3.2, and the sustainment capabilities of this system are described in Chapter 9.

Improved Li coverage: NSTX CHI discharges routinely relied on Li evaporative coatings on the lower divertor tiles to reduce the influx of oxygen impurities. However, during final weeks of CHI discharge improvements on NSTX, the lower divertor tiles were only partly coated with Li as only one of the lower divertor Li evaporator was functional. NXTX-U CHI discharges will benefit from dual Li evaporators to coat the lower divertor tiles more completely. This is expected to further reduce the oxygen influx into the CHI discharge. In addition, NSTX-U will also have a Li evaporator to coat the upper divertor tiles. This should be particularly helpful during absorber arcs, as Li instead of oxygen will be primary species injected into the CHI plasma. Because of both these systems the resulting CHI discharges could be expected to have a higher intrinsic electron temperature and a higher plasma current magnitude. The Li evaporator system is described under Section 10.5.2.5

Higher CHI voltage capability: Results from the HIT-II experiment show that by optimizing the injector voltage, injector flux and toroidal field, the extent of closed flux current can be

increased. To increase the closed flux current more injector flux is needed. To reduce the injector current at higher levels of injector flux, the toroidal field needs to be increased. At higher toroidal field, the injector voltage needs to be increased.

On NSTX, such an optimization was not possible as during the final three years of NSTX operations the capacitor bank was essentially operated at its highest voltage of 1.7 kV, as reducing the voltage reduced the achievable plasma current. The present voltage snubbing system on the CHI system (the Metal Oxide Varistors) begins to significantly conduct at a voltage of 1.7 kV. In order to extend the voltage to the full 2 kV that the CHI capacitor bank system is capable of, new MOVs with a higher voltage rating are required. The higher voltage also allows the injector current pulse width to be reduced. Shorter pulse width CHI discharges would have less impurity influx from the injector and from the absorber. Thus CHI voltage, which is a very powerful control variable, has not been exercised on NSTX. NSTX-U itself is being designed for 4kV CHI capability, which is a factor of two higher than the 2kV capability of NSTX. On NSTX-U a staged approach will be used to increase the CHI capacitor bank voltage to at least 2.5 kV, and possibly as high as 3 kV.

The present CHI power supply consists of up to ten capacitors, each 5 mF in capacitance. Any number of these can be connected in parallel and discharged. During Years 1 and 2 of NSTX-U operations, the voltage capability of the MOVs will be increased so that the CHI capacitor bank can be operated at the full 2 kV level it was designed for. The staged capability that allows a smaller portion of the capacitor bank to be discharged at different times will be used. The maximum bank size will be 50 mF at 2 kV and it will have the capability for three staged operations (i.e., the bank can be broken into three parts and each part can be individually triggered).

Based on the results from these experiments, during Year 3, new upgrades will be implemented. First, the capacitor bank voltage will be increased to 3 kV. Simultaneously the MOVs will be upgraded to handle the higher voltage. The staged capability will be increased to four stages.

Metallic divertor plates: During plasma start-up, whether it is inductive or CHI start-up, low-Z impurities need to be reduced in magnitude. At the low electron temperature of start-up plasmas, impurities such as carbon and oxygen can radiate heavily and keep the plasma temperature from increasing. During plasma start-up using an electrode discharge process such as CHI it is preferable to have metallic electrodes, as metallic impurities do no radiated heavily until the electron temperature generally exceeds about 100 eV. All spheromak experiments that generated high electron temperature plasma (over 100 eV) relied on metallic electrodes. During Year 3 of NSTX-U operations, NSTX-U plans to replace the graphite divertor plates with tiles fabricated out of refractory element. This upgrade is described in Section 10.5.2.6. These, in addition to the other upgrades mentioned above should work synergistically and help to significantly increase the intrinsic CHI plasma electron temperature and current magnitude.

In summary, the successful demonstration on NSTX of CHI start-up, and subsequent ramp-up to 1 MA when induction applied in combination with the major upgrades in NSTX-U (higher toroidal field, 2nd NBI system for additional power and more tangential injection, and a 1 MW ECH system) combined with density reduction that is possible with CHI generated seed current plasmas, NSTX-U is well positioned for a demonstration of full non-inductive current start-up and ramp-up to 1MA in support of a FNSF.

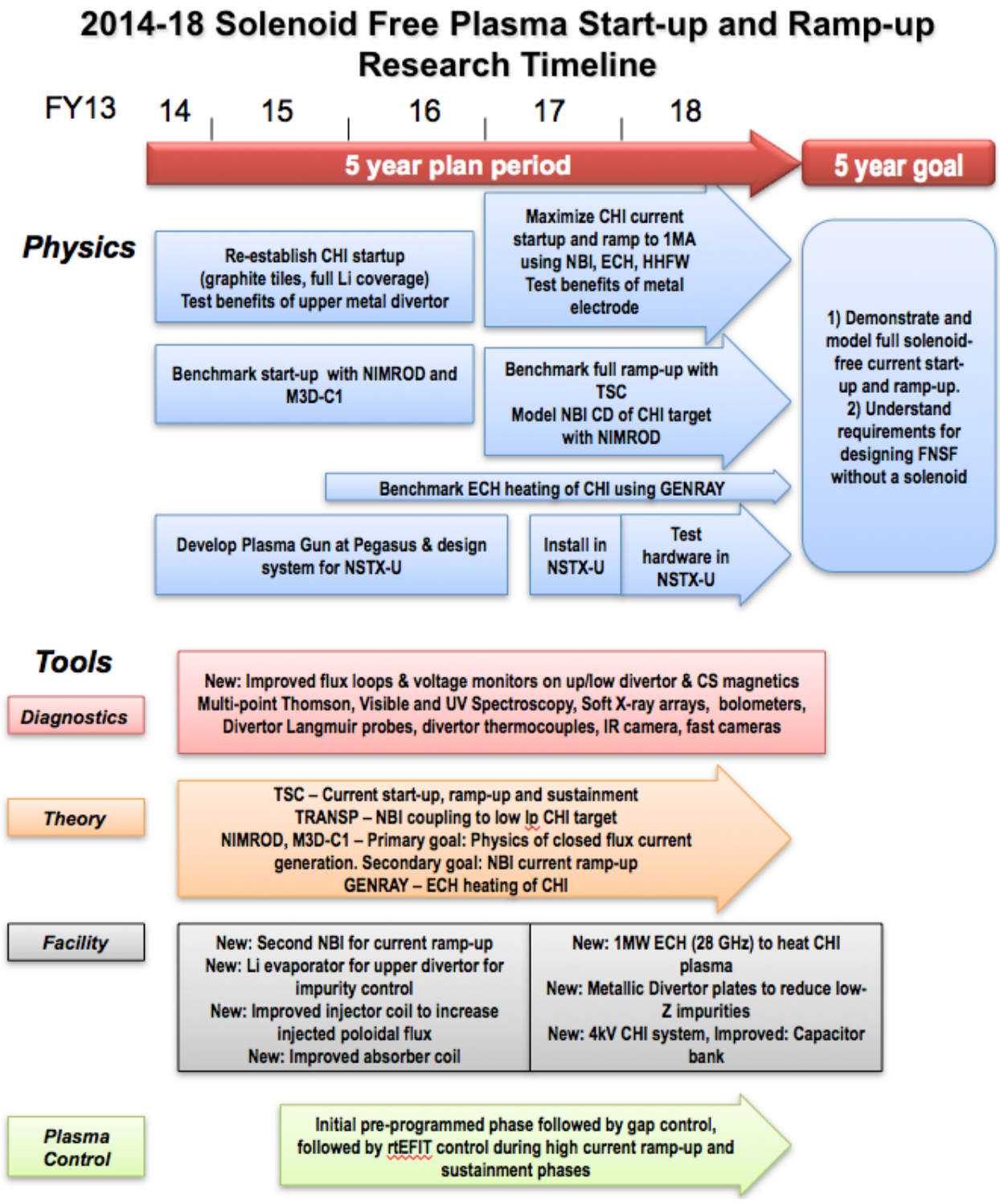
2014-18 Solenoid Free Plasma Start-up and Ramp-up Research Timeline
FY13
14
15
16
17
18
5 year plan period
5 year goal
Physics
Re-establish CHI startup (graphite tiles, full Li coverage) Test benefits of upper metal divertor
Maximize CHI current startup and ramp to 1MA using NBI, ECH, HHFW Test benefits of metal electrode
Benchmark start-up with NIMROD and M3D-C1
Benchmark full ramp-up with TSC Model NBI CD of CHI target with NIMROD
Benchmark ECH heating of CHI using GENRAY
Develop Plasma Gun at Pegasus & design system for NSTX-U
Install in NSTX-U
Test hardware in NSTX-U
1) Demonstrate and model full solenoid-free current start-up and ramp-up. 2) Understand requirements for designing FNSF without a solenoid
Tools
Diagnostics
New: Improved flux loops & voltage monitors on up/low divertor & CS magnetics Multi-point Thomson, Visible and UV Spectroscopy, Soft X-ray arrays, bolometers, Divertor Langmuir probes, divertor thermocouples, IR camera, fast cameras
Theory
TSC – Current start-up, ramp-up and sustainment
TRANSP – NBI coupling to low Ip CHI target
NIMROD, M3D-C1 – Primary goal: Physics of closed flux current generation. Secondary goal: NBI current ramp-up
GENRAY – ECH heating of CHI
Facility
New: Second NBI for current ramp-up
New: Li evaporator for upper divertor for impurity control
New: Improved injector coil to increase injected poloidal flux
New: Improved absorber coil
New: 1MW ECH (28 GHz) to heat CHI plasma
New: Metallic Divertor plates to reduce low-Z impurities
New: 4kV CHI system, Improved: Capacitor bank
Plasma Control
Initial pre-programmed phase followed by gap control, followed by rtEFIT control during high current ramp-up and sustainment phases

References

[1] See references 13-18 in Chapter 1
[2] V.F. Shevchenko et al., Nucl. Fusion **50** (2010) 022004
[3] G. Taylor et al., Phys. of Plasmas **19** (2012) 045001
[4] R. Raman, T.R. Jarboe, B.A. Nelson, et al., Phys. Rev. Lett., **90**, 075005 (2003)
[5] R. Raman, B.A. Nelson, M.G. Bell, et al., Phys. Rev. Lett., **97**, 175002 (2006)
[6] D. Mueller, B.A. Nelson, W.T. Hamp, et al., Phys. Plasmas, **12** (7) 070702 (2005)
[7] T.R. Jarboe, Plasma Phys. Control. Fusion **36**, 945 (1994)
[8] C.W. Barnes, T.R. Jarboe, et al., Phys. Fluids **B 2**, 1871 (1990)
[9] H.S. McLean, et al., Phys. Rev. Lett. **88**, 125004 (2002)
[10] C.W. Barnes, J.C. Fernandez, I. Henins, et al., Phys. Fluids **29**, 3415 (1986)
[11] J.H. Hammer et al., Phys. Fluids B **3**, 2236 (1991)
[12] Y. Ono et al., Phys. Rev. Lett. **76**, 3328 (1996)
[13] M. Nagata et al., Phys. Plasmas **10**, 2932 (2003)
[14] R. Raman, T.R. Jarboe, D. Mueller et al., Plasma Phys. Control. Fusion **43**, 305 (2001)
[15] R. Raman, T.R. Jarboe, D. Mueller, et al., Nucl. Fusion **41**, 1081 (2001)
[16] R. Raman, T. R. Jarboe, W.T. Hamp, Physics of Plasmas, **14**, 022504 (2007)
[17] R. Raman, D. Mueller, B.A. Nelson, Phys. Rev. Lett., **104**, 095003 (2010)
[18] N.W. Eidietis, R.J. Fonck, G.D. Garstka, et al., J. Fusion Energy, 26, 43 (2007) doi: 10.1007/s10894-006-9072-z
[19] G. Fiksel, A. F. Almagri, D. Craig, et al., Plasma Sources Sci. Technol. **5**, 78 (1996).
[20] D. Den Hartog, D. Craig, G. Fiksel, and J. Sarff, Plasma Sources Sci. Technol. **6**, 492 (1997)
[21] D.J. Bataglia, M.W. Bongard, R.J. Fonck, et al., Phys. Rev. Letter **102**, 225003 (2009)
[22] A.J. Redd, et al., APS DPP (2012) **PP8 24**, Providence, Rhode island
[23] T.R. Jarboe, B.S. Victor, B.A. Nelson, et al., Nuclear Fusion **52**, 083017 (2012)
[24] R. Raman, D. Mueller, T.R. Jarboe, et al., Physics of Plasmas **18**, 092504 (2011)
[25] B.A. Nelson, T.R. Jarboe, D. Mueller, R. Raman, et al., Nuclear Fusion **51**, 063008 (2011)
[26] J.E. Menard, et al. Nuclear Fusion **52**, (2012) 083051
[27] T.R. Jarboe, Fusion Tech. **15**, 7 (1989)
[28] R. Raman, T.R. Jarboe, R.G. O'Neill, et al., Nuclear Fusion - Letter, **45**, L15-L19 (2005)
[29] A.J. Redd, et al., APS DPP (2011) **B04 14**, Salt Lake City, Utah
[30] R.J. Fonck, et al., APS DPP (2012) **GO6 10**, Providence, Rhode Island
[31] J.B. Taylor, Reviews of Modern Physics **58**, 741 (1986)
[32] H. W. Kugel, et al., Physics of Plasmas **15**, 056118 (2008)
[33] R. Raman, S.C. Jardin, J. Menard, et al., Nuclear Fusion **51**, 113018 (2011)
[34] F. Scotti et al., Rev. Sci. Instrum. **83**, 10E532 (2012)
[35] S.C. Jardin, C.E. Kessel, N. Pomphrey, Nucl. Fusion, **34**, 8, (1994)
[36] S.C. Jardin, M.G. Bell, N. Pomphrey, Nucl. Fusion, **33**, 371 (1993)
[37] C. R. Sovinec, A. H. Glasser, T. A. Gianakon, et al. J. Comput. Phys **195**, 355 (2004)
[38] C. R. Sovinec, D. D. Schnack, A. Y. Pankin, et al., J. Physics: Conference Series **16**, 25 (IoP, London, 2005)
[39] C. C. Kim, C. R. Sovinec, S. E. Parker, and the NIMROD Team, Computer Physics

Communications **164**, 448 (2004)
[40] E. D. Held, J. D. Callen, C. C. Hegna, et al., Phys. Plasma **11**, 2419 (2004)
[41] T. G. Jenkins, S. E. Kruger, C. C. Hegna, et al., Physics of Plasmas **17**, 12502 (2010)
[42] J. B. O'Bryan, C. R. Sovinec, and T. M Bird, Physics of Plasmas **19**, 080701 (2012)
[43] N. M. Ferraro, et al., Phys. Plasmas **17** (2010) 102508
[44] N. M. Ferraro, et al., Phys. Plasmas **19** (2012) 056105
[45] A. P. Smirnov and R.W. Harvey, Bull. Am. Phys. Soc. **40**, 1837 (1995)
[46] A. P. Smirnov, et al., Proc. 15th Workshop on ECE and ECRH, (World Scientific, 2009), p. 301